Journal of Computational Physics 230 (2011) 2977–2996

Contents lists available at ScienceDirect

Journal of Computational Physics

journal homepage: www.elsevier.com/locate/jcp

Approximation of the inductionless MHD problem using a stabilized finite element method

Ramon Planas *, Santiago Badia, Ramon Codina

Centre Internacional de Mètodes Numèrics en Enginyeria (CIMNE), Universitat Politècnica de Catalunya, Jordi Girona 1-3, Edifici C1, 08034 Barcelona, Spain

ARTICLE INFO

Article history:
Received 2 August 2010
Received in revised form 14 December 2010
Accepted 25 December 2010
Available online 14 January 2011

Keywords:
Inductionless MHD
Primal–dual formulation
Stabilized finite element formulation
Variational multiscale method
Monolithic scheme
HCLL test blanket module

ABSTRACT

In this work, we present a stabilized formulation to solve the inductionless magnetohydrodynamic (MHD) problem using the finite element (FE) method. The MHD problem couples the Navier–Stokes equations and a Darcy-type system for the electric potential via Lorentz's force in the momentum equation of the Navier–Stokes equations and the currents generated by the moving fluid in Ohm's law. The key feature of the FE formulation resides in the design of the stabilization terms, which serve several purposes. First, the formulation is suitable for convection dominated flows. Second, there is no need to use interpolation spaces constrained to a compatibility condition in both sub-problems and therefore, equal-order interpolation spaces can be used for all the unknowns. Finally, this formulation leads to a coupled linear system; this monolithic approach is effective, since the coupling can be dealt by effective preconditioning and iterative solvers that allows to deal with high Hartmann numbers.

1. Introduction

The objective of this work is to present a finite element (FE) method for the approximation of the inductionless magnetohydrodynamic (MHD) problem which arises when the magnetic field induced by currents in the liquid metal is negligible compared to the external magnetic field, $\boldsymbol{B}$. The inductionless approximation to the MHD problem consists of the momentum, mass and charge conservation equations together with Ohm's law; the problem is written in terms of velocity $\boldsymbol{u}$, pressure p, current density $\boldsymbol{j}$ and electric potential ϕ. The structure of this system of partial differential equations corresponds to the Navier–Stokes equations coupled to a Darcy-type problem via Lorentz's force and generated currents terms.

This set of equations can be used to model several industrial processes, such as MHD pumps based on conduction or induction principles, MHD generators, continuous casting of steel, crystal growth devices or test blanket modules (TBMs) in nuclear fusion reactors. TBMs will be one of the key components of International Thermonuclear Experimental Reactor (ITER), that should demonstrate the scientific reliability of fusion (see <www.iter.org> for more details). Each of these breeding blankets is designed in a modular shape performing a triple function: (1) heat power extraction from the plasma, (2) tritium generation (breeding) and (3) shielding of the magnets from neutron and gamma radiation. The breeding material used is the eutectic lead–lithium liquid metal. In normal regimes, this liquid metal flow can be modeled by the inductionless MHD equations. The aim to design effective TBMs and the lack of experimental data has increased the demand of numerical methods for this system of equations.

The FE approximation of the inductionless MHD system faces several difficulties. First, there is the classical and well-known problem of dealing with cases in which the first order derivatives, i.e. the convective term in the Navier–Stokes

* Corresponding author.
E-mail address: rplanas@cimne.upc.edu (R. Planas).

0021-9991/$ - see front matter © 2011 Elsevier Inc. All rights reserved.
doi:10.1016/j.jcp.2010.12.046

equations, dominate the second order ones, i.e. the viscous term. In this singular limit, the elliptic nature of the system of differential equations vanishes. This behavior may lead to oscillations when using crude Galerkin techniques. Second, there is the compatibility condition between the approximation spaces for the velocity and the pressure, but also for the current density and the electric potential. These conditions are expressed in a classical inf-sup form. Finally, the coupling between the hydrodynamic and the electromagnetic problems may lead to numerical difficulties when solving the resulting discrete system of equations. In the Navier–Stokes equations, the coupling comes from Lorentz's force, whereas in the magnetic problem the coupling appears in Ohm's law because the conducting fluid moves with velocity $\boldsymbol{u}$. The goal of this work is to design a stabilized FE method able to circumvent all these problems.

The stabilization technique presented in this work is developed in the variational multiscale framework introduced in [18]. It is based on a two-scale decomposition of the unknowns into a FE component and a subgrid scale or subscale that corresponds to the unknown component that can not be captured by the FE space. The key ingredient is the model for the subgrid scales. In this work, we have considered the subgrid scales as a projection of the residual of the FE approximation times a matrix of stabilization parameters. Among the several options for the projection and the structure of the matrix of stabilization parameters, the identity and a diagonal structure have been chosen, respectively. Up to this point, the only missing issue to close the formulation is the design of the stabilization parameters. Based on the stability and convergence analyses of the method, we have obtained an effective expression for them.

In the last years, the increasing demand of computational tools for the design on fusion reactor technology has increased the interest on computational MHD. However, the literature about the numerical approximation of the inductionless MHD equations is still quite scarce. There has been some recent research done in the finite difference and finite volume community. The finite volume method has been used to solve the inductionless MHD equations in simulations of the HCLL test blanket module in nuclear fusion reactors (see, e.g., [6,21] for examples in this field). In all cases, the methodology consists of first solving a Poisson equation for the electric potential (obtained by taking the divergence of the Ohm's law) and then, solving the Navier–Stokes equations adding the Lorentz force as a body force in the momentum equation. A crude fixed point iterative algorithm is used to converge to the coupled solution. Using this approach, a conservative finite volume scheme for incompressible MHD flows is proposed in [24,25]; the scheme further uncouples the computation of velocities and pressures via a pressure segregation scheme; see, e.g., [1,10] for a detailed exposition of pressure segregation schemes and the quite poor performance of fixed point iterations over the $\boldsymbol{u}$-p resulting system. Since block Jacobi and block Gauss–Seidel preconditioned Richardson iterations converge in a quite poor fashion (when convergence is attained), more effective preconditioned solvers are mandatory for large scale simulations (see, e.g., [15]). This observation motivates the monolithic approach proposed herein; the scheme we propose ends up with a linear system that couples the fluid and magnetic problems. The coupling can be transferred to the preconditioner in an effective manner and then an efficient and robust iterative solver (like GMRES) can be used, leading to optimal MHD solvers. In this work, we have considered incomplete LU factorizations of the monolithic system as preconditioners, together with a GMRES iterative solver.

There exist several articles applying the FE method to solve the full MHD equations in the general case of non-negligible induced magnetic field (see for instance [12,17,28–30]) but the authors are not aware of previous works dealing with the approximation of the inductionless MHD by the FE method. For this work, we have used the same methodology as for the full MHD problem in [11], treating the same issues with a similar strategy, even though the problems considered are significantly different from the point of view of the mathematical structure.

The article is organized as follows. The problem to be solved is stated in Section 2, both in its continuous and its variational form. Issues regarding the time integration and the linearization of the nonlinear term are discussed in Section 3, leading to a time discrete and linearized scheme. Next, the variational multiscale framework is applied to the inductionless MHD problem in Section 4. After proposing the stabilization method, it is fully analyzed regarding its stability, accuracy and convergence properties; it motivates an optimal expression of the stabilization parameters that takes into account the coupling. The final scheme proposed in this work is written in Section 5. Numerical experiments verifying the theoretical results are presented in Section 6 and finally, some conclusions are drawn in Section 7.

2. Problem statement

2.1. Initial and boundary value problem

Let $\Omega \subset \mathbb{R}^d$ ($d = 2$ or 3) be a domain where we want to solve the inductionless MHD problem during the time interval $[0,T]$. The unknowns of the problem are the fluid velocity $\boldsymbol{u} : \Omega \times (0,T) \to \mathbb{R}^d$, the pressure $p : \Omega \times (0,T) \to \mathbb{R}$, the current density $\boldsymbol{j} : \Omega \times (0,T) \to \mathbb{R}^d$ and the electric potential $\phi : \Omega \times (0,T) \to \mathbb{R}$, which are the solution of the system of partial differential equations:

$$\partial_t \boldsymbol{u} + \boldsymbol{u} \cdot \nabla \boldsymbol{u} - \nu \Delta \boldsymbol{u} + \nabla p - \frac{1}{\rho}(\boldsymbol{j} \times \boldsymbol{B}) = \boldsymbol{f}, \tag{1}$$

$$\nabla \cdot \boldsymbol{u} = 0, \tag{2}$$

$$\boldsymbol{j} + \sigma \nabla \phi - \sigma(\boldsymbol{u} \times \boldsymbol{B}) = 0, \tag{3}$$

$$\nabla \cdot \boldsymbol{j} = 0, \tag{4}$$

where ρ is the fluid density, $\boldsymbol{B}$ the external magnetic field, $\boldsymbol{f}$ the body forces of the flow motion and σ the electric conductivity. It is important to note that the pressure p we are working with here is the kinematic pressure (pressure divided by density).

Let us define two different partitions of the domain boundary $\Gamma = \partial\Omega$. The first one, for imposing the boundary conditions of the hydrodynamic unknowns, is divided into the part $\Gamma_{E,u}$ in which essential (Dirichlet) boundary conditions are enforced, and the rest of the boundary $\Gamma_{N,u}$ where we impose natural (Neumann) boundary conditions. The other partition is used for the boundary conditions of the magnetic problem. It consists of the part of the boundary $\Gamma_{C,j}$ that corresponds to perfectly conducting walls and the part $\Gamma_{I,j}$ that corresponds to perfectly insulated walls. So, we have:

$$\Gamma = \Gamma_{E,u} \cup \Gamma_{N,u} = \Gamma_{C,j} \cup \Gamma_{I,j}, \quad \text{and} \quad \emptyset = \Gamma_{E,u} \cap \Gamma_{N,u} = \Gamma_{C,j} \cap \Gamma_{I,j}.$$

The boundary conditions for the velocity at the walls are the non-slip wall conditions, that is to say, $\boldsymbol{u} = \boldsymbol{0}$ on $\Gamma_{E,u}$. On the other hand, the free boundary conditions for the velocity are zero traction conditions,

$$-p\boldsymbol{n} + \nu\boldsymbol{n} \cdot \nabla\boldsymbol{u} = 0, \quad \text{on} \quad \Gamma_{N,u}.$$

Two different kinds of boundary conditions have been considered for the magnetic equations. For insulating walls, the electric currents cannot cross the wall surface, which implies that the normal component of the density currents has to vanish, that is, $\boldsymbol{j} \cdot \boldsymbol{n} = 0$ on $\Gamma_{I,j}$. On the other hand, perfectly conducting walls do not apply any resistance to the current and therefore, the electric currents cross the wall surface in an orthogonal way. This means that the tangential component of the density current has to vanish on the boundary, i.e. $\boldsymbol{j} \times \boldsymbol{n} = \boldsymbol{0}$ on $\Gamma_{C,j}$. Note that, because $\boldsymbol{u} = \boldsymbol{0}$ on the wall boundary, the density current and the electric potential are related as $\boldsymbol{j} = -\sigma\nabla\phi$. Therefore, on a perfectly conducting wall it is verified that $\nabla\phi \times \boldsymbol{n} = 0$. This means that ϕ must be constant on the boundary. So, we can model conducting walls by the boundary condition $\phi = 0$ on $\Gamma_{C,j}$ without loss of generality.

Finally, an initial condition for the velocity field has to be considered, i.e. $\boldsymbol{u} = \boldsymbol{u_0}$ in Ω at instant $t = 0$.

2.2. Weak form

Let us introduce some notation. Let $<f,g>_\omega := \int_\omega fg$, where f and g are two generic functions defined on a region ω such that the integral of their product is well defined. When $f, g \in L^2(\Omega)$, we will write $(f,g)_\omega := <f, g>_\omega$. The norm in $L^2(\Omega)$ will be denoted by $\|f\| := (f,f)^{1/2}$.

Let $\boldsymbol{v}, q, \boldsymbol{k}$ and ψ be the test functions for $\boldsymbol{u}, p, \boldsymbol{j}$ and ϕ, respectively. We consider them time-independent because time will be discretized using a finite difference scheme. To obtain the weak form of (1)–(4), the equations are multiplied by the corresponding test functions, integrated over the domain Ω and the second order terms are integrated by parts, resulting in the variational form

$$(\partial_t\boldsymbol{u}, \boldsymbol{v}) + \langle \boldsymbol{u} \cdot \nabla\boldsymbol{u}, \boldsymbol{v}\rangle + \nu(\nabla\boldsymbol{u}, \nabla\boldsymbol{v}) - (p, \nabla \cdot \boldsymbol{v}) - \frac{1}{\rho}\langle \boldsymbol{j} \times \boldsymbol{B}, \boldsymbol{v}\rangle = \langle \boldsymbol{f}, \boldsymbol{v}\rangle, \tag{5}$$

$$(q, \nabla \cdot \boldsymbol{u}) = 0, \tag{6}$$

$$(\boldsymbol{j}, \boldsymbol{k}) + \sigma(\nabla\phi, \boldsymbol{k}) - \sigma(\boldsymbol{u} \times \boldsymbol{B}, \boldsymbol{k}) = 0, \tag{7}$$

$$-(\nabla\psi, \boldsymbol{j}) = -\langle \psi, \boldsymbol{j} \cdot \boldsymbol{n}\rangle_\Gamma, \tag{8}$$

which must hold for all test functions $\boldsymbol{v}$, q, $\boldsymbol{k}$ and ψ in the functional spaces that will be defined next. Note that σ is assumed to be constant and that the boundary term appearing from integration by parts in (8) is zero both in the case of conducting walls and in the case of insulating walls. Let us assume that $\boldsymbol{B} \in L^3(\Omega)$, in order for this system to be well-posed in the subsequent functional setting. The functional spaces considered in this work are

$$V_u = \left\{ \boldsymbol{v} \in H^1(\Omega)^d \middle| \boldsymbol{v} = \boldsymbol{0} \text{ on } \Gamma_{E,u} \right\},$$

$$V_p = \left\{ q \in L^2(\Omega) \middle| \int_\Omega q = 0 \text{ if } \Gamma_{N,u} = \emptyset \right\},$$

$$V_j = \left\{ \boldsymbol{k} \in L^2(\Omega)^d \middle| \boldsymbol{k} \cdot \boldsymbol{n} = 0 \text{ on } \Gamma_{I,j} \right\},$$

$$V_\phi = \left\{ \psi \in H^1(\Omega) \middle| \psi = 0 \text{ on } \Gamma_{C,j} \right\}.$$

Remark 1. It is important to note that the $\boldsymbol{j}$-ϕ system has the same structure as the Darcy problem. The formulation selected in this work corresponds to the primal version of the problem. However, there exists also the dual formulation which consists of considering a different functional setting of the problem: $\boldsymbol{j} \in H(\mathrm{div};\Omega)$ and $\phi \in L^2(\Omega)$, see [2] for a complete definition and stabilized FE analysis of these two formulations for Darcy's problem.

Remark 2. From (3), it follows that the trace of $\boldsymbol{j} \cdot \boldsymbol{n}$ is well defined if so is the trace of $\boldsymbol{n} \cdot \nabla\phi$ and $\boldsymbol{n} \cdot (\boldsymbol{u} \times \boldsymbol{B}) = (\boldsymbol{n} \times \boldsymbol{B}) \cdot \boldsymbol{u}$. The first term is well defined because $\phi \in H^1(\Omega)$. The second term is well-defined for $\boldsymbol{B} \in H(\mathrm{curl};\Omega)$ (e.g., for $\boldsymbol{B}$ a given datum solving the Maxwell equations), since $\boldsymbol{u} \in H^1(\Omega)^d$ has trace on $\Gamma_{I,j}$ (for almost all t).

The multilinear forms appearing in the variational form of the problem are well defined and continuous for

$$\begin{aligned}
&\boldsymbol{u} \in L^2(0,T;V_u), \quad \boldsymbol{v} \in V_u,\\
&p \in \mathcal{D}'(0,T;V_p), \quad q \in V_p,\\
&\boldsymbol{j} \in \mathcal{D}'(0,T;V_j), \quad \boldsymbol{k} \in V_j,\\
&\phi \in \mathcal{D}'(0,T;V_\phi), \quad \psi \in V_\phi.
\end{aligned}$$

In these expressions, the Bochner space $L^2(0,T;X)$ denotes the set of mappings defined on $\Omega \times (0,T)$ such that their X-spatial norm is an $L^2(0,T)$ function. Similarly, $\mathcal{D}'(0,T;X)$ denotes the set of mappings for which their X-spatial norm is a distribution in time.

The variational form of the problem (5)–(8) can be written as a single variational equation of the form

$$M(\partial_t \boldsymbol{U}, \boldsymbol{V}) + A(\boldsymbol{U}, \boldsymbol{V}) = L(\boldsymbol{V}), \tag{9}$$

where

$$\begin{aligned}
&\boldsymbol{U} := [\boldsymbol{u}, p, \boldsymbol{j}, \phi]^t, \quad \boldsymbol{V} := [\boldsymbol{v}, q, \boldsymbol{k}, \psi]^t,\\
&A(\boldsymbol{U}, \boldsymbol{V}) := \langle (\boldsymbol{u}\cdot\nabla)\boldsymbol{u}, \boldsymbol{v}\rangle + \nu(\nabla\boldsymbol{u}, \nabla\boldsymbol{v}) - (p, \nabla\cdot\boldsymbol{v}) + (q, \nabla\cdot\boldsymbol{u}) - \frac{1}{\rho}\langle \boldsymbol{j}\times\boldsymbol{B}, \boldsymbol{v}\rangle\\
&\qquad + \alpha_j[(\boldsymbol{j}, \boldsymbol{k}) + \sigma(\nabla\phi, \boldsymbol{k}) - \sigma(\boldsymbol{u}\times\boldsymbol{B}, \boldsymbol{k})] + \alpha_\phi[-(\nabla\psi, \boldsymbol{j})],\\
&L(\boldsymbol{V}) := \langle \boldsymbol{f}, \boldsymbol{v}\rangle,\\
&M(\boldsymbol{U}, \boldsymbol{V}) := (\boldsymbol{u}, \boldsymbol{v}).
\end{aligned}$$

The scaling coefficients α_j and α_ϕ are introduced to make $A(\boldsymbol{U},\boldsymbol{U})$ dimensionally consistent. A possible choice of these coefficients is

$$\alpha_j = \frac{1}{\rho\sigma}, \quad \alpha_\phi = \frac{1}{\rho}.$$

3. Linearization, time discretization and spatial approximation

3.1. Linearization of the stationary inductionless MHD problem

The simplest way to linearize problem (9) is by a fixed point method, i.e. Picard's method. Let us assume there exists an estimate for the velocity at iteration k, $\boldsymbol{u}^k$. Then the approximation of $A(\boldsymbol{U},\boldsymbol{V})$ at iteration $k+1$ using Picard's method can be written as

$$\begin{aligned}
A^{k+1}(\boldsymbol{U}^{k+1}, \boldsymbol{V}) = {}& \langle (\boldsymbol{u}^k\cdot\nabla)\boldsymbol{u}^{k+1}, \boldsymbol{v}\rangle + \nu(\nabla\boldsymbol{u}^{k+1}, \nabla\boldsymbol{v}) - (p^{k+1}, \nabla\cdot\boldsymbol{v}) + (q, \nabla\cdot\boldsymbol{u}^{k+1}) - \frac{1}{\rho}\left\langle \boldsymbol{j}^{k+1}\times\boldsymbol{B}, \boldsymbol{v}\right\rangle + \frac{1}{\rho\sigma}(\boldsymbol{j}^{k+1}, \boldsymbol{k})\\
&+ \frac{1}{\rho}(\nabla\phi^{k+1}, \boldsymbol{k}) - \frac{1}{\rho}(\boldsymbol{u}^{k+1}\times\boldsymbol{B}, \boldsymbol{k}) - \frac{1}{\rho}(\nabla\psi, \boldsymbol{j}^{k+1}).
\end{aligned}$$

Remark 3. Note that the linearization proposed above is the only one that leads to a stable scheme that satisfies an energy bound. It comes from the fact that testing the linearized system with $\mathbf{v} = \boldsymbol{u}^{k+1}$ and $\boldsymbol{k} = \boldsymbol{j}^{k+1}$, the coupling terms cancel out:

$$-\frac{1}{\rho}\langle \boldsymbol{j}^{k+1}\times\boldsymbol{B}, \boldsymbol{u}^{k+1}\rangle - \frac{1}{\rho}(\boldsymbol{u}^{k+1}\times\boldsymbol{B}, \boldsymbol{j}^{k+1}) = 0.$$

Analogously, we can easily check that a $\boldsymbol{u}-\phi$ formulation in which ϕ is computed using a Poisson problem and $\boldsymbol{j}$ is recovered as a postprocess cannot lead to a stable algorithm satisfying an energy inequality. This is one of the reasons that favor the choice of a $\boldsymbol{u}-\boldsymbol{j}$ formulation. It implies that the problem needs to be solved for $\boldsymbol{u}^{k+1}$, p^{k+1}, $\boldsymbol{j}^{k+1}$ and ϕ^{k+1} in a coupled way. Then, it is very convenient to have all the unknowns in terms of their nodal values, i.e. equal order Lagrangian FE approximations of all the components of the vectorial quantities and scalar quantities, which reinforces the choice of a monolithic approach to solve the problem.

Therefore, calling $\boldsymbol{a} \equiv \boldsymbol{u}^k$, $\boldsymbol{u} \equiv \boldsymbol{u}^{k+1}$, $p \equiv p^{k+1}$, $\boldsymbol{j} \equiv \boldsymbol{j}^{k+1}$ and $\phi \equiv \phi^{k+1}$, the linearization of the stationary inductionless MHD scaled problem is

$$\begin{aligned}
&-\nu\Delta\boldsymbol{u} + \boldsymbol{a}\cdot\nabla\boldsymbol{u} + \nabla p - \frac{1}{\rho}(\boldsymbol{j}\times\boldsymbol{B}) = \boldsymbol{f},\\
&\nabla\cdot\boldsymbol{u} = 0,
\end{aligned}$$

$$\frac{1}{\rho\sigma}\boldsymbol{j}+\frac{1}{\rho}\nabla\phi-\frac{1}{\rho}(\boldsymbol{u}\times\boldsymbol{B})=0,$$
$$\frac{1}{\rho}\nabla\cdot\boldsymbol{j}=0.$$

The linearized counterpart of the variational form (9) is written as

$$M(\partial_t\boldsymbol{U},\boldsymbol{V})+A^{\mathrm{lin}}(\boldsymbol{U},\boldsymbol{V})=L(\boldsymbol{V}), \tag{10}$$

where

$$A^{\mathrm{lin}}(\boldsymbol{U},\boldsymbol{V})=\nu(\nabla\boldsymbol{u},\nabla\boldsymbol{v})+\langle\boldsymbol{a}\cdot\nabla\boldsymbol{u},\boldsymbol{v}\rangle-(p,\nabla\cdot\boldsymbol{v})+(q,\nabla\cdot\boldsymbol{u})-\frac{1}{\rho}\langle\boldsymbol{j}\times\boldsymbol{B},\boldsymbol{v}\rangle+\frac{1}{\rho\sigma}(\boldsymbol{j},\boldsymbol{k})+\frac{1}{\rho}(\nabla\phi,\boldsymbol{k})$$
$$-\frac{1}{\rho}(\boldsymbol{u}\times\boldsymbol{B},\boldsymbol{k})-\frac{1}{\rho}(\nabla\psi,\boldsymbol{j}).$$

3.2. Stability of the continuous and linearized problem

Consider the linearized stationary problem. Its variational form is: Find the solution $\boldsymbol{U}\in(V_u\times V_p\times V_j\times V_\phi)$ of the problem

$$A^{\mathrm{lin}}(\boldsymbol{U},\boldsymbol{V})=L(\boldsymbol{V})\quad\forall\boldsymbol{V}\in(V_u\times V_p\times V_j\times V_\phi). \tag{11}$$

Note that, since $\nabla\cdot\boldsymbol{a}=0$ at the continuous level, A^{lin} satisfies the stability estimate

$$A^{\mathrm{lin}}(\boldsymbol{U},\boldsymbol{U})=\nu\|\nabla\boldsymbol{u}\|^2+\frac{1}{\rho\sigma}\|\boldsymbol{j}\|^2. \tag{12}$$

In order to be able to guarantee that the linearized problem is well posed, the inf-sup conditions between V_u and V_p and between V_j and V_ϕ have to be added to the stability estimate given by (12); we refer to [5,16] for a detailed exposition of these concepts. For the inductionless MHD problem, the corresponding inf-sup conditions are

$$\inf_{q\in V_p}\sup_{\boldsymbol{v}\in V_u}\frac{(q,\nabla\cdot\boldsymbol{v})}{\|q\|\|\nabla\boldsymbol{v}\|}\geqslant\beta^*>0,\qquad\inf_{\psi\in V_\phi}\sup_{\boldsymbol{k}\in V_j}\frac{(\nabla\psi,\boldsymbol{k})}{\|\nabla\psi\|\|\boldsymbol{k}\|}\geqslant\gamma^*>0,$$

where β^* and γ^* are positive constants. Therefore, for each iteration k and given $\boldsymbol{u}^k$, there exists a unique solution $(\boldsymbol{u}^{k+1},p^{k+1},\boldsymbol{j}^{k+1},\phi^{k+1})$ of the linearized problem (11).

3.3. Time discretization of the linearized scheme

Consider the variational problem given by (10) and a uniform partition of the time domain $[0,T]$ of size δt, the time step size. The method used in this work for the time integration is

$$M(\delta_t\boldsymbol{U}^n,\boldsymbol{V})+A^{\mathrm{lin}}(\boldsymbol{U}^{n+1},\boldsymbol{V})=L(\boldsymbol{V}),$$

where $\delta_t\boldsymbol{U}^n=\delta t^{-1}(\boldsymbol{U}^{n+1}-\boldsymbol{U}^n)$. This time discretization corresponds to the Backward-Euler method, which is a first-order method in time. Other time integration schemes could also be applied to obtain the final discrete problem, e.g., the second order Crank–Nicholson scheme. Anyway, the following discussion can straightforwardly be extended to other time integration schemes.

The time discrete and linearized scheme reads as:

For $n=0,1,2,\ldots,T/\delta t$, given $\boldsymbol{u}^n$ find $\boldsymbol{u}^{n+1}$, p^{n+1}, $\boldsymbol{j}^{n+1}$ and ϕ^{n+1} as the converged solutions of the following iterative algorithm, initialized with the values at the previous time step n:

$$(\delta_t\boldsymbol{u}^{n,k+1},\boldsymbol{v})+\langle(\boldsymbol{u}^{n+1,k}\cdot\nabla)\boldsymbol{u}^{n+1,k+1},\boldsymbol{v}\rangle+\nu(\nabla\boldsymbol{u}^{n+1,k+1},\nabla\boldsymbol{v})-(p^{n+1,k+1},\nabla\cdot\boldsymbol{v})$$
$$-\frac{1}{\rho}\langle\boldsymbol{j}^{n+1,k+1}\times\boldsymbol{B},\boldsymbol{v}\rangle=\langle\boldsymbol{f}^{\,n+1},\boldsymbol{v}\rangle, \tag{13}$$
$$(q,\nabla\cdot\boldsymbol{u}^{n+1,k+1})=0, \tag{14}$$
$$\frac{1}{\rho\sigma}(\boldsymbol{j}^{n+1,k+1},\boldsymbol{k})+\frac{1}{\rho}(\nabla\phi^{n+1,k+1},\boldsymbol{k})-\frac{1}{\rho}(\boldsymbol{u}^{n+1,k+1}\times\boldsymbol{B},\boldsymbol{k})=0, \tag{15}$$
$$-\frac{1}{\rho}(\nabla\psi,\boldsymbol{j}^{n+1,k+1})=0, \tag{16}$$

where $k>0$ is the iteration counter. Therefore, considering $\boldsymbol{a}\equiv\boldsymbol{u}^{n+1,k}$, $\boldsymbol{u}\equiv\boldsymbol{u}^{n+1,k+1}$, $p\equiv p^{n+1,k+1}$, $\boldsymbol{j}\equiv\boldsymbol{j}^{n+1,k+1}$ and $\phi\equiv\phi^{n+1,k+1}$, the differential equations associated to (13)–(16) are

$$\delta_t \boldsymbol{u} - \nu\Delta\boldsymbol{u} + \boldsymbol{a}\cdot\nabla\boldsymbol{u} + \nabla p - \frac{1}{\rho}(\boldsymbol{j}\times\boldsymbol{B}) = \boldsymbol{f},$$

$$\nabla\cdot\boldsymbol{u} = 0,$$

$$\frac{1}{\rho\sigma}\boldsymbol{j} + \frac{1}{\rho}\nabla\phi - \frac{1}{\rho}(\boldsymbol{u}\times\boldsymbol{B}) = 0,$$

$$\frac{1}{\rho}\nabla\cdot\boldsymbol{j} = 0.$$

This problem can be written as the vector differential equation

$$\boldsymbol{M}\delta_t\boldsymbol{U} + \mathcal{L}(\boldsymbol{U}) = \boldsymbol{F} \quad \text{in}\Omega, \tag{17}$$

where $\boldsymbol{M} = \text{diag}\,(\boldsymbol{I},0,\boldsymbol{0},0)$, $\boldsymbol{I}$ being the $d\times d$ identity, $\delta_t\boldsymbol{U} = (\delta t)^{-1}(\boldsymbol{U}-\boldsymbol{U}^n)$, $\boldsymbol{F} = [\boldsymbol{f},0,\boldsymbol{0},0]^t$ a vector of $n_{\text{unk}} = 2d+2$ components and the scaled operator $\mathcal{L}$ is given by

$$\mathcal{L}(\boldsymbol{U}) = \begin{bmatrix} -\nu\Delta\boldsymbol{u} + \boldsymbol{a}\cdot\nabla\boldsymbol{u} + \nabla p - \frac{1}{\rho}(\boldsymbol{j}\times\boldsymbol{B}) \\ \nabla\cdot\boldsymbol{u} \\ \frac{1}{\rho\sigma}\boldsymbol{j} + \frac{1}{\rho}\nabla\phi - \frac{1}{\rho}(\boldsymbol{u}\times\boldsymbol{B}) \\ \frac{1}{\rho}\nabla\cdot\boldsymbol{j} \end{bmatrix}. \tag{18}$$

The time discrete and linearized version of the variational form (9) can be written as

$$M(\delta_t\boldsymbol{U},\boldsymbol{V}) + A^{\text{lin}}(\boldsymbol{U},\boldsymbol{V}) = L(\boldsymbol{V}). \tag{19}$$

3.4. Space discretization and stability of the Galerkin approximation

The space discretization of problem (19) is obtained by means of the classical Galerkin FE approximation. Therefore, the problem can be stated as:

Given $\boldsymbol{U}_h^n$, find $\boldsymbol{U}_h \in (V_{u,h}\times V_{p,h}\times V_{j,h}\times V_{\phi,h})$ such that

$$M(\delta_t\boldsymbol{U}_h,\boldsymbol{V}_h) + A^{\text{lin}}(\boldsymbol{U}_h,\boldsymbol{V}_h) = L(\boldsymbol{V}_h) \quad \forall\boldsymbol{V}_h \in (V_{u,h}\times V_{p,h}\times V_{j,h}\times V_{\phi,h}), \tag{20}$$

where the FE spaces $V_{u,h}$, $V_{p,h}$, $V_{j,h}$ and $V_{\phi,h}$ are subspaces of their infinite dimensional counterparts V_u, V_p, V_j and V_ϕ (i.e., a conforming approximation is considered).

The Galerkin approximation of the inductionless MHD problem satisfies the stability estimate

$$A^{\text{lin}}(\boldsymbol{U}_h,\boldsymbol{U}_h) = \nu\|\nabla\boldsymbol{u}_h\|^2 + \frac{1}{\rho\sigma}\|\boldsymbol{j}_h\|^2. \tag{21}$$

Remark 4. We have assumed here that $\nabla\cdot\boldsymbol{a} = 0$. This is not necessarily true at the discrete level, where $\boldsymbol{a} = \boldsymbol{u}_h^{n+1,k}$. Technically speaking, we should work with the skew-symmetric expression of the convective term, $(\boldsymbol{u}\cdot\nabla)\boldsymbol{u} + \frac{1}{2}(\nabla\cdot\boldsymbol{u})\boldsymbol{u}$. However, the results obtained in the numerical analysis of the stabilized formulation would be the same. Therefore, we will keep working with the assumption $\nabla\cdot\boldsymbol{a} = 0$ for simplicity. We refer to [3] for the technicalities associated to the use of the skew-symmetric form.

The stability given by estimate (21) is not enough to guarantee that the discrete problem is well-posed. Thus, discrete inf-sup conditions between $V_{u,h}$ and $V_{p,h}$ and between $V_{j,h}$ and $V_{\phi,h}$ have to be satisfied. The corresponding discrete inf-sup conditions are

$$\inf_{q_h\in V_{p,h}}\sup_{\boldsymbol{v}_h\in V_{u,h}}\frac{(q_h,\nabla\cdot\boldsymbol{v}_h)}{\|q_h\|\|\nabla\boldsymbol{v}_h\|} \geqslant \beta^* > 0, \quad \inf_{\psi_h\in V_{\phi,h}}\sup_{\boldsymbol{k}_h\in V_{j,h}}\frac{(\nabla\psi_h,\boldsymbol{k}_h)}{\|\nabla\psi_h\|\|\boldsymbol{k}_h\|} \geqslant \gamma^* > 0, \tag{22}$$

where β^* and γ^* are positive constants uniform with respect to the mesh size h and different from the constants appearing in the inf-sup conditions for the continuous problem.

The Galerkin FE approximation of this problem faces several well-known difficulties. First, oscillations may appear when dealing with problems where the first order derivatives dominate the second order derivatives in the Navier–Stokes equations. Second, the compatibility conditions being verified at the continuous level do not imply that the discrete versions will also be verified. It depends on the choice of the FE spaces $V_{u,h}$, $V_{p,h}$, $V_{j,h}$ and $V_{\phi,h}$. For instance, equal order approximation spaces $V_{u,h}$ and $V_{p,h}$ or $V_{j,h}$ and $V_{\phi,h}$ do not verify the discrete inf-sup conditions. Finally, when the coupling between the hydrodynamical and the electromagnetic problems is strong, the solution of the discrete system of equations may lead to

numerical difficulties. The approach taken in this work to face these difficulties is the use of a stabilization method able to deal with all these drawbacks of the Galerkin FE approximation.

4. Stabilized formulation and numerical analysis

4.1. Stabilized FE approximation for the linearized problem

The basic idea of the stabilization method proposed in this work is based on the subgrid scale concept introduced in [18]. The following ideas are a summary of the approach described in [8]. The main idea is to split the continuous solution of the problem in two components, the FE solution and the *subscales* or *subgrid scales*, which are the part of the solution that cannot be captured by the discretization. In this situation, the problem is reduced to obtain a good approximation for the *subscales*.

There exist several subgrid scale (SGS) stabilization methods. The purpose of this paper is to see how to apply a well established formulation to the inductionless MHD problem. This can be obtained by approximating the subscales by the algebraic expression

$$\widetilde{\boldsymbol{U}} \approx \boldsymbol{\tau}\widetilde{P}[\boldsymbol{F} - \mathcal{L}(\boldsymbol{U}_h)], \tag{23}$$

where $\boldsymbol{\tau}$ is a $n_{unk} \times n_{unk}$ matrix of stabilization parameters, the expression of which is discussed below, and $\widetilde{P}$ is the projection onto the space of subscales. The option taken in this work has been $\widetilde{P} = I$, the identity, although it is also possible to take $\widetilde{P} = P_h^{\perp}$, the projection orthogonal to the final element space; we refer to [9,26] for a discussion about the benefits of this last approach. Herein, we have used $\widetilde{P} = I$ for simplicity and because it is the most widely used option in the variational multiscale community. Anyway, the statement of the orthogonal subscales method is straightforward.

The discrete problem to be solved is: Find $\boldsymbol{U}_h \in (V_{u,h} \times V_{p,h} \times V_{j,h} \times V_{\phi,h})$ such that

$$A^{\text{lin}}_{\text{stab}}(\boldsymbol{U}_h, \boldsymbol{V}_h) = L_{\text{stab}}(\boldsymbol{V}_h) \quad \forall \boldsymbol{V}_h \in (V_{u,h} \times V_{p,h} \times V_{j,h} \times V_{\phi,h})$$

where

$$A^{\text{lin}}_{\text{stab}}(\boldsymbol{U}_h, \boldsymbol{V}_h) = A^{\text{lin}} - \langle \mathcal{L}^*(\boldsymbol{V}_h), \boldsymbol{\tau}\mathcal{L}(\boldsymbol{U}_h)\rangle_h, \tag{24}$$

$$L_{\text{stab}}(\boldsymbol{V}_h) = L(\boldsymbol{V}_h) - \langle \mathcal{L}^*(\boldsymbol{V}_h), \boldsymbol{\tau}\boldsymbol{F}\rangle_h, \tag{25}$$

and where the notation

$$\langle \cdot, \cdot \rangle_h := \sum_{e=1}^{n_{el}} \langle \cdot, \cdot \rangle_{\Omega^e},$$

has been used. The adjoint operator of this problem $\mathcal{L}^*(\boldsymbol{V}_h)$ is given by

$$\mathcal{L}^*(\boldsymbol{V}_h) = \begin{bmatrix} -\nu\Delta\boldsymbol{v}_h - \boldsymbol{a}\cdot\nabla\boldsymbol{v}_h - \nabla q_h + \frac{1}{\rho}(\boldsymbol{k}_h \times \boldsymbol{B}) \\ -\nabla\cdot\boldsymbol{v}_h \\ \frac{1}{\rho\sigma}\boldsymbol{k}_h - \frac{1}{\rho}\nabla\psi_h + \frac{1}{\rho}(\boldsymbol{v}_h \times \boldsymbol{B}) \\ -\frac{1}{\rho}\nabla\cdot\boldsymbol{k}_h \end{bmatrix}. \tag{26}$$

The next step is to define an expression for the matrix of stabilization parameters $\boldsymbol{\tau}$. In the case we are considering, we will see in the following subsection that stability can be improved maintaining optimal accuracy by taking a diagonal expression for $\boldsymbol{\tau}$, with one scalar component for each equation. In the 3D case we have

$$\boldsymbol{\tau} = \text{diag}(\tau_1, \tau_1, \tau_1, \tau_2, \tau_3, \tau_3, \tau_3, \tau_4). \tag{27}$$

Using both expressions (26) and (27) in problem (24) and (25), the stabilized bilinear form is

$$\begin{aligned} A^{\text{lin}}_{\text{stab}}(\boldsymbol{U}_h, \boldsymbol{V}_h) &= A^{\text{lin}}(\boldsymbol{U}_h, \boldsymbol{V}_h) - \langle \mathcal{L}^*(\boldsymbol{V}_h), \boldsymbol{\tau}\mathcal{L}(\boldsymbol{U}_h)\rangle_h \\ &= A^{\text{lin}}(\boldsymbol{U}_h, \boldsymbol{V}_h) + \langle X_u(\boldsymbol{v}_h, q_h, \boldsymbol{k}_h) + \nu\Delta\boldsymbol{v}_h, \tau_1(X_u(\boldsymbol{u}_h, p_h, \boldsymbol{j}_h) - \nu\Delta\boldsymbol{u}_h)\rangle_h + \langle \nabla\cdot\boldsymbol{v}_h, \tau_2(\nabla\cdot\boldsymbol{u}_h)\rangle_h \\ &\quad + \left\langle X_j(\boldsymbol{v}_h, \psi_h) - \frac{1}{\rho\sigma}\boldsymbol{k}_h, \tau_3\left(X_j(\boldsymbol{u}_h, \phi_h) + \frac{1}{\rho\sigma}\boldsymbol{j}_h\right)\right\rangle_h + \left\langle \frac{1}{\rho}\nabla\cdot\boldsymbol{k}_h, \tau_4\left(\frac{1}{\rho}\nabla\cdot\boldsymbol{j}_h\right)\right\rangle_h, \end{aligned} \tag{28}$$

where we have used the abbreviations

$$X_u(\boldsymbol{v}_h, q_h, \boldsymbol{k}_h) := \boldsymbol{a}\cdot\nabla\boldsymbol{v}_h + \nabla q_h - \frac{1}{\rho}(\boldsymbol{k}_h \times \boldsymbol{B}),$$

$$X_j(\boldsymbol{v}_h, \psi_h) := \frac{1}{\rho}\nabla\psi_h - \frac{1}{\rho}(\boldsymbol{v}_h \times \boldsymbol{B}).$$

The right-hand-side of the stabilized problem is given by

$$L_{\text{stab}}(\boldsymbol{V}_h) = L(\boldsymbol{V}_h) - \langle \mathcal{L}^*(\boldsymbol{V}_h), \boldsymbol{\tau F})\rangle_h = L(\boldsymbol{V}_h) + \langle X_u(\boldsymbol{v}_h, q_h, \boldsymbol{k}_h) + \nu\Delta\boldsymbol{v}_h, \tau_1\boldsymbol{f}\rangle_h.$$

The definition of the stabilized FE method only misses the expression of the stabilization parameters. The expressions proposed in this work are

$$\begin{aligned}
&\alpha := c_1\frac{a}{h} + c_2\frac{\nu}{h^2}, \quad \beta := c_3\frac{B}{\rho}, \quad \gamma := c_4\frac{1}{\rho\sigma},\\
&\tau_1 = \alpha^{-1}\left(1 + \frac{1}{\sqrt{\alpha\gamma}}\beta\right)^{-1}, \quad \tau_2 = c_5\frac{h^2}{\tau_1},\\
&\tau_3 = \gamma^{-1}\left(1 + \frac{1}{\sqrt{\alpha\gamma}}\beta\right)^{-1}, \quad \tau_4 = c_6\frac{\rho^2h^2}{\tau_3}.
\end{aligned} \tag{29}$$

These expressions are evaluated element by element. Here, a is the maximum norm of the velocity field $\boldsymbol{a}$ computed in the element under consideration. Likewise, B is the maximum norm of the magnetic field $\boldsymbol{B}$ in the corresponding element, and h the element diameter.

The stabilization parameters have been developed for the steady problem. For the transient problem, we consider the stabilized formulation

$$M(\delta_t\boldsymbol{U}_h, \boldsymbol{V}_h) + A^{\text{lin}}_{\text{stab}}(\boldsymbol{U}_h, \boldsymbol{V}_h) = L_{\text{stab}}(\boldsymbol{V}_h) \quad \forall \boldsymbol{V}_h \in (V_{u,h} \times V_{p,h} \times V_{j,h} \times V_{\phi,h}),$$

instead of (20). Therefore, the stabilization parameters are the same as those of the steady problem and do not depend on the time step size.[1] Alternatively, in order to take into account the time behavior of the subscale, we could consider *dynamic* subscales (see [13]). For the sake of conciseness, we have not included this option here, but it is straightforward from the quasi-static formulation above and [13].

Note that if $-\mathcal{L}^*(\boldsymbol{V}_h)$ is replaced by $\mathcal{L}(\boldsymbol{V}_h)$ (which amounts for a change in two signs), a GLS formulation of the induction-less MHD problem is recovered [19].

4.2. Numerical analysis and justification of the stabilization parameters

In this subsection we proceed with the numerical analysis of the formulation introduced before that will justify the stabilization parameter expression (29). For the sake of simplicity we assume that $\boldsymbol{a}$ and $\boldsymbol{B}$ are constant and that the FE meshes are quasi-uniform. Thus, we can consider a characteristic mesh size h in the definition of the stabilization parameters and therefore τ_i, $i = 1, 2, 3, 4$ are constant. Moreover, for quasi-uniform meshes the following inverse estimates hold

$$\|\nabla v_h\| \leqslant \frac{C_{\text{inv}}}{h}\|v_h\|, \quad \|\nabla\nabla v_h\| \leqslant \frac{C_{\text{inv}}}{h}\|\nabla v_h\|, \tag{30}$$

for any function v_h in the FE space and for a certain constant C_{inv}.

The stability and convergence analysis will be made using the mesh-dependent norm

$$\begin{aligned}
|||\boldsymbol{U}_h|||^2 :=\ & \nu\|\nabla\boldsymbol{u}_h\|^2 + \frac{1}{\rho\sigma}\|\boldsymbol{j}_h\|^2 + \tau_1\|\boldsymbol{a}\cdot\nabla\boldsymbol{u}_h + \nabla p_h - \frac{1}{\rho}(\boldsymbol{j}_h\times\boldsymbol{B})\|^2 + \tau_2\|\nabla\cdot\boldsymbol{u}_h\|^2 + \tau_3\|\frac{1}{\rho}\nabla\phi_h - \frac{1}{\rho}(\boldsymbol{u}_h\times\boldsymbol{B})\|^2\\
&+ \tau_4\frac{1}{\rho^2}\|\nabla\cdot\boldsymbol{j}_h\|^2 = \nu\|\nabla\boldsymbol{u}_h\|^2 + \frac{1}{\rho\sigma}\|\boldsymbol{j}_h\|^2 + \tau_1\|X_u(\boldsymbol{u}_h, p_h, \boldsymbol{j}_h)\|^2 + \tau_2\|\nabla\cdot\boldsymbol{u}_h\|^2 + \tau_3\|X_j(\boldsymbol{u}_h, \phi_h)\|^2\\
&+ \tau_4\frac{1}{\rho^2}\|\nabla\cdot\boldsymbol{j}_h\|^2.
\end{aligned} \tag{31}$$

From now on, C will denote a positive constant independent of the mesh discretization and the physical parameters, not necessarily the same at different stages.

4.2.1. Coercivity

Let us start by proving stability in the form of coercivity of the bilinear form (28):

$$\begin{aligned}
A^{\text{lin}}_{\text{stab}}(\boldsymbol{U}_h, \boldsymbol{U}_h) = A^{\text{lin}}(\boldsymbol{U}_h, \boldsymbol{U}_h) - \langle\mathcal{L}^*(\boldsymbol{U}_h), \boldsymbol{\tau}\mathcal{L}(\boldsymbol{U}_h)\rangle_h =\ & \nu\|\nabla\boldsymbol{u}_h\|^2 + \frac{1}{\rho\sigma}\|\boldsymbol{j}_h\|^2 + \tau_1\|X_u(\boldsymbol{u}_h, p_h, \boldsymbol{j}_h)\|^2 - \tau_1\nu^2\|\Delta\boldsymbol{u}_h\|^2\\
&+ \tau_2\|\nabla\cdot\boldsymbol{u}_h\|^2 + \tau_3\|X_j(\boldsymbol{u}_h, \phi_h)\|^2 - \tau_3\frac{1}{\rho^2\sigma^2}\|\boldsymbol{j}_h\|^2 + \tau_4\frac{1}{\rho^2}\|\nabla\cdot\boldsymbol{j}_h\|^2.
\end{aligned}$$

Using the second inverse estimate in (30), a sufficient condition for $A^{\text{lin}}_{\text{stab}}$ to be coercive is

[1] This kind of stabilized transient formulation is the *quasi-static* subscale approach in [13]. Therein, we have justified why time step size dependent stabilization parameters should be avoided.

$$\nu - \tau_1 \nu^2 \frac{C_{\text{inv}}^2}{h^2} \geqslant \alpha\nu \iff \tau_1 \leqslant (1-\alpha)\frac{1}{\nu}\frac{h^2}{C_{\text{inv}}^2}, \tag{32}$$

$$\frac{1}{\rho\sigma} - \tau_3 \frac{1}{\rho^2\sigma^2} \geqslant \alpha\frac{1}{\rho\sigma} \iff \tau_3 \leqslant (1-\alpha)\rho\sigma, \tag{33}$$

with $0 < \alpha < 1$. Conditions (32) and (33) imply

$$A_{\text{stab}}^{\text{lin}}(\boldsymbol{U}_h, \boldsymbol{U}_h) \geqslant C|||\boldsymbol{U}_h|||^2,$$

for a constant C independent of the discretization and of the physical parameters.

4.2.2. Optimal accuracy

The requirement that the stabilized formulation is optimally accurate will allow us to obtain new conditions on the stabilization parameters. These new conditions together with (32) and (33) from stability will lead to the final expression of the stabilization parameters.

For a function v, let $\pi_h(v)$ be its optimal FE approximation. We assume that the following estimates hold

$$\|v - \pi_h(v)\|_{H^i(\Omega)} \leqslant \varepsilon_i(v) := Ch^{k+1-i}|v|_{H^{k+1}(\Omega)}, \quad i = 0, 1, \tag{34}$$

where $\|v\|_{H^q(\Omega}$ is the $H^q(\Omega)$-norm of v, that is, the sum of the $L^2(\Omega)$-norm of the derivatives of v up to degree q, $|v|_{H^q(\Omega)}$ the corresponding semi-norm, and k the degree of the FE approximation.

We will prove next that the interpolation error function of the formulation is

$$E(h) := \tau_1^{-1/2}\varepsilon_0(\boldsymbol{u}) + \tau_2^{-1/2}\varepsilon_0(p) + \tau_3^{-1/2}\varepsilon_0(\boldsymbol{j}) + \tau_4^{-1/2}\varepsilon_0(\phi).$$

Let $\boldsymbol{U}$ be the solution of the continuous problem and $\pi_h(\boldsymbol{U})$ its optimal FE approximation. The accuracy estimate that will be needed to prove convergence is

$$A_{\text{stab}}^{\text{lin}}(\boldsymbol{U} - \pi_h(\boldsymbol{U}), \boldsymbol{V}_h) \leqslant CE(h)|||\boldsymbol{V}_h|||, \tag{35}$$

for any FE function $\boldsymbol{V}_h$.

Let us prove this by showing that both the Galerkin and the stabilization terms in $A_{\text{stab}}^{\text{lin}}$ satisfy estimate (35) for sufficiently smooth solutions of the continuous problem. Integrating by parts some terms in the Galerkin contribution we obtain

$$\begin{aligned} A^{\text{lin}}(\boldsymbol{U} - \pi_h(\boldsymbol{U}), \boldsymbol{V}_h) &= \nu(\nabla(\boldsymbol{u} - \pi_h(\boldsymbol{u})), \nabla\boldsymbol{v}_h) - (\boldsymbol{u} - \pi_h(\boldsymbol{u}), \boldsymbol{a}\cdot\nabla\boldsymbol{v}_h) - (\boldsymbol{u} - \pi_h(\boldsymbol{u}), \nabla q_h) - (p - \pi_h(p), \nabla\cdot\boldsymbol{v}_h) \\ &+ \frac{1}{\rho}(\boldsymbol{u} - \pi_h(\boldsymbol{u}), \boldsymbol{k}_h \times \boldsymbol{B}) + \frac{1}{\rho}(\boldsymbol{j} - \pi_h(\boldsymbol{j}), \boldsymbol{v}_h \times \boldsymbol{B}) + \frac{1}{\rho\sigma}(\boldsymbol{j} - \pi_h(\boldsymbol{j}), \boldsymbol{k}_h) - \frac{1}{\rho}(\boldsymbol{j} - \pi_h(\boldsymbol{j}), \nabla\psi_h) \\ &+ \frac{1}{\rho}(\nu\nabla\cdot(\boldsymbol{u} - \pi_h(\boldsymbol{u})), \nabla\cdot\boldsymbol{k}_h) \leqslant C\Big(\varepsilon_0(\boldsymbol{u})\tau_1^{-1/2}\tau_1^{1/2}\|\nu\Delta(\boldsymbol{u} - \pi_h(\boldsymbol{u}))\| + \varepsilon_0(p)\tau_2^{-1/2}\tau_2^{1/2}\|\nabla\cdot\boldsymbol{v}_h\| \\ &+ \varepsilon_0(\boldsymbol{u})\tau_2^{-1/2}\tau_2^{1/2}\|\boldsymbol{a}\cdot\nabla\boldsymbol{v}_h\| + \varepsilon_0(\boldsymbol{u})\tau_3^{-1/2}\tau_3^{1/2}\|\nabla q_h\| + \varepsilon_0(\boldsymbol{j})\tau_3^{-1/2}\tau_3^{1/2}\|\boldsymbol{k}_h\| \\ &+ \varepsilon_0(\boldsymbol{u})\tau_4^{-1/2}\tau_4^{1/2}\frac{1}{\rho}\|\boldsymbol{B}\times\boldsymbol{k}_h\| + \varepsilon_0(\boldsymbol{j})\tau_4^{-1/2}\tau_4^{1/2}\frac{1}{\rho}\|\boldsymbol{v}_h\times\boldsymbol{B}\| + \varepsilon_0(\boldsymbol{j})\tau_3^{-1/2}\tau_3^{1/2}\frac{1}{\rho\sigma}\|\boldsymbol{k}_h\| \\ &+ \varepsilon_0(\boldsymbol{j})\tau_4^{-1/2}\tau_4^{1/2}\frac{1}{\rho}\|\nabla\psi_h\| + \varepsilon_0(\boldsymbol{u})\tau_1^{-1/2}\tau_1^{1/2}\frac{1}{\rho}\|\nu\nabla\cdot\boldsymbol{k}_h\| + \varepsilon_0(\boldsymbol{j})\tau_2^{-1/2}\tau_2^{1/2}\frac{1}{\rho}\|\nabla\cdot\boldsymbol{k}_h\| \\ &\times\nabla\cdot\boldsymbol{v}_h\| + \varepsilon_0(\boldsymbol{j})\tau_3^{-1/2}\tau_3^{1/2}\left[\|X_j(\boldsymbol{v}_h, \psi_h)\| + \frac{1}{\rho\sigma}\|\boldsymbol{k}_h\|\right] + \varepsilon_0(\phi)\tau_4^{-1/2}\tau_4^{1/2}\frac{1}{\rho}\|\nabla\cdot\boldsymbol{k}_h\|\Big). \end{aligned} \tag{36}$$

Conditions (32) and (33) and the expression of the interpolation errors imply

$$\nu^{1/2}\varepsilon_1(\boldsymbol{u}) \leqslant C\varepsilon_0(\boldsymbol{u})\tau_1^{-1/2}, \quad \frac{1}{(\rho\sigma)^{1/2}}\|\boldsymbol{k}_h\| \leqslant \tau_3^{-1/2}\|\boldsymbol{k}_h\|,$$

and therefore from (36) it follows that the Galerkin contribution to $A_{\text{stab}}^{\text{lin}}(\boldsymbol{U} - \pi_h(\boldsymbol{U}), \boldsymbol{V}_h)$ can be bounded as indicated in (35). It remains to prove that also the stabilization terms can be bounded the same way:

$$\begin{aligned} -\langle\mathcal{L}^*(\boldsymbol{V}_h), \boldsymbol{\tau}\mathcal{L}(\boldsymbol{U} - \pi_h(\boldsymbol{U}))\rangle_h &= \langle X_u(\boldsymbol{v}_h, q_h, \boldsymbol{k}_h) + \nu\Delta\boldsymbol{v}_h, \tau_1(X_u(\boldsymbol{u} - \pi_h(\boldsymbol{u}), p - \pi_h(p), \boldsymbol{j} - \pi_h(\boldsymbol{j})) - \nu\Delta(\boldsymbol{u} - \pi_h(\boldsymbol{u})))\rangle_h \\ &+ \langle\nabla\cdot\boldsymbol{v}_h, \tau_2\nabla\cdot(\boldsymbol{u} - \pi_h(\boldsymbol{u}))\rangle_h + \left\langle\frac{1}{\rho}\nabla\cdot\boldsymbol{k}_h, \tau_4\frac{1}{\rho}\nabla\cdot(\boldsymbol{j} - \pi_h(\boldsymbol{j}))\right\rangle_h \\ &+ \left\langle X_j(\boldsymbol{v}_h, \psi_h) - \frac{1}{\rho\sigma}\boldsymbol{k}_h, \tau_3(X_j(\boldsymbol{u} - \pi_h(\boldsymbol{u}), \phi - \pi_h(\phi)) + \frac{1}{\rho\sigma}(\boldsymbol{j} - \pi_h(\boldsymbol{j})))\right\rangle_h \\ &\leqslant C\left(\tau_1^{1/2}\|X_u(\boldsymbol{u} - \pi_h(\boldsymbol{u}), p - \pi_h(p), \boldsymbol{j} - \pi_h(\boldsymbol{j}))\| + \tau_1^{1/2}\nu\|\Delta(\boldsymbol{u} - \pi_h(\boldsymbol{u}))\|\right) \\ &\times\left(|||\boldsymbol{V}_h||| + \tau_1^{1/2}\nu\|\Delta\boldsymbol{v}_h\|\right) + C\tau_2^{1/2}\varepsilon_1(\boldsymbol{u})|||\boldsymbol{V}_h||| + C\tau_4^{1/2}\frac{1}{\rho}\varepsilon_1(\boldsymbol{j})|||\boldsymbol{V}_h||| \\ &+ C\left(\tau_3^{1/2}\|X_j(\boldsymbol{u} - \pi_h(\boldsymbol{u}), \phi - \pi_h(\phi))\| + \tau_3^{1/2}\frac{1}{\rho\sigma}(\boldsymbol{j} - \pi_h(\boldsymbol{j}))\right) \\ &\times\left(|||\boldsymbol{V}_h||| + \tau_3^{1/2}\frac{1}{\rho\sigma}\|\boldsymbol{k}_h\|\right). \end{aligned} \tag{37}$$

Using again conditions (32) and (33) and the inverse estimates (30) we have

$$\tau_1^{1/2}\nu\|\Delta\boldsymbol{v}_h\| \leqslant C\tau_1^{1/2}\nu^{1/2}\frac{C_{\text{inv}}}{h}\|\nabla\boldsymbol{v}_h\| \leqslant C|||\boldsymbol{V}_h|||,$$
$$\tau_3^{1/2}\frac{1}{\rho\sigma}\|\boldsymbol{k}_h\| \leqslant C(\rho\sigma)^{1/2}\frac{1}{\rho\sigma}\|\boldsymbol{k}_h\| \leqslant C|||\boldsymbol{V}_h|||.$$

Therefore, we get from (37) that

$$\begin{aligned}-\langle\mathcal{L}^*(\boldsymbol{V}_h),\boldsymbol{\tau}\mathcal{L}(\boldsymbol{U}-\pi_h(\boldsymbol{U}))\rangle_h &\leqslant C|||\boldsymbol{V}_h|||\left[\tau_1^{1/2}\left(\frac{\nu}{h^2}\varepsilon_0(\boldsymbol{u})+\frac{a}{h}\varepsilon_0(\boldsymbol{u})+\frac{1}{h}\varepsilon_0(p)+\frac{B}{\rho}\varepsilon_0(\boldsymbol{j})\right)+\tau_2^{1/2}\left(\frac{1}{h}\varepsilon_0(\boldsymbol{u})\right)\right.\\ &\quad\left.+\tau_3^{1/2}\left(\frac{1}{\rho\sigma}\varepsilon_0(\boldsymbol{j})+\frac{1}{\rho h}\varepsilon_0(\phi)+\frac{B}{\rho}\varepsilon_0(\boldsymbol{u})\right)+\tau_4^{1/2}\left(\frac{1}{\rho h}\varepsilon_0(\boldsymbol{j})\right)\right]\\ &\leqslant C|||\boldsymbol{V}_h|||\left[\varepsilon_0(\boldsymbol{u})\left[\tau_1^{1/2}\left(\frac{\nu}{h^2}+\frac{a}{h}\right)+\tau_2^{1/2}\frac{1}{h}+\tau_3^{1/2}\frac{B}{\rho}\right]+\varepsilon_0(p)\left[\tau_1^{1/2}\frac{1}{h}\right]\right.\\ &\quad\left.+\varepsilon_0(\boldsymbol{j})\left[\tau_1^{1/2}\frac{B}{\rho}+\tau_3^{1/2}\frac{1}{\rho\sigma}+\tau_4^{1/2}\frac{1}{\rho h}\right]+\varepsilon_0(\phi)\left[\tau_3^{1/2}\frac{1}{\rho h}\right]\right].\end{aligned}$$

Using the definition (29) of the stabilization parameters it is easily checked that these terms can also be bounded as indicated in (35).

Remark 5. The last step provides the crucial design condition for the stabilization parameters. Expressions (29) result from solving

$$\tau_1^{1/2}\left(\frac{\nu}{h^2}+\frac{a}{h}\right)+\tau_2^{1/2}\frac{1}{h}+\tau_3^{1/2}\frac{B}{\rho}\sim\tau_1^{-1/2}, \tag{38}$$
$$\tau_1^{1/2}\frac{1}{h}\sim\tau_2^{-1/2}, \tag{39}$$
$$\tau_1^{1/2}\frac{B}{\rho}+\tau_3^{1/2}\frac{1}{\rho\sigma}+\tau_4^{1/2}\frac{1}{\rho h}\sim\tau_3^{-1/2}, \tag{40}$$
$$\tau_3^{1/2}\frac{1}{\rho h}\sim\tau_4^{-1/2}, \tag{41}$$

where $\sim$ stands for equality up to constants that do not depend on the physical variables nor the mesh discretization.

4.2.3. Convergence

The properties of stability and optimal accuracy, in the sense of (35) allow us to show that the method is optimally convergent. From the orthogonality property $A^{\text{lin}}_{\text{stab}}(\boldsymbol{U}-\boldsymbol{U}_h,\boldsymbol{V}_h)=0$ for any FE function $\boldsymbol{V}_h$, a consequence of the consistency of the method, we have that

$$\begin{aligned}C|||\pi_h(\boldsymbol{U})-\boldsymbol{U}_h|||^2 &\leqslant A^{\text{lin}}_{\text{stab}}(\pi_h(\boldsymbol{U})-\boldsymbol{U}_h,\pi_h(\boldsymbol{U})-\boldsymbol{U}_h) \leqslant A^{\text{lin}}_{\text{stab}}(\pi_h(\boldsymbol{U})-\boldsymbol{U},\pi_h(\boldsymbol{U})-\boldsymbol{U}_h)+A^{\text{lin}}_{\text{stab}}(\boldsymbol{U}-\boldsymbol{U}_h,\pi_h(\boldsymbol{U})-\boldsymbol{U}_h)\\ &\leqslant CE(h)|||\pi_h(\boldsymbol{U})-\boldsymbol{U}_h|||,\end{aligned}$$

and so $|||\pi_h(\boldsymbol{U})-\boldsymbol{U}_h||| \leqslant C\,E(h)$. If we apply the triangle inequality, we get

$$|||\boldsymbol{U}-\boldsymbol{U}_h||| \leqslant |||\boldsymbol{U}-\pi_h(\boldsymbol{U})||| + |||\pi_h(\boldsymbol{U})-\boldsymbol{U}_h||| \leqslant |||\boldsymbol{U}-\pi_h(\boldsymbol{U})||| + CE(h).$$

It is trivial to check that $|||\boldsymbol{U}-\pi_h(\boldsymbol{U})||| \leqslant C\,E(h)$ using the expression of the norm (31), the interpolation estimates (34) and the stabilization parameters (29). Therefore,

$$|||\boldsymbol{U}-\boldsymbol{U}_h||| \leqslant CE(h).$$

The fact that this error estimate is exactly the same as the estimate for the interpolation error $|||\boldsymbol{U}-\pi_h(\boldsymbol{U})||| \leqslant C\,E(h)$ justifies why it can be considered optimal.

5. Final numerical scheme

The final numerical scheme proposed to solve the inductionless MHD problem results from applying the stabilized FE approximation described in Section 4.1 to the time discrete and linearized problem (13)–(16). Therefore, the final algorithm

reads: For $n = 0,1,2,\ldots, T/\delta t$ and given $\boldsymbol{u}^n$, find $\boldsymbol{u}^{n+1}$, p^{n+1}, $\boldsymbol{j}^{n+1}$ and ϕ^{n+1} as the converged solutions of the following iterative algorithm:

$$
\begin{aligned}
&(\delta_t \boldsymbol{u}_h^{n,k+1}, \boldsymbol{v}_h) + \left\langle (\boldsymbol{u}_h^{n+1,k}\cdot\nabla)\boldsymbol{u}_h^{n+1,k+1}, \boldsymbol{v}_h \right\rangle + \nu(\nabla \boldsymbol{u}_h^{n+1,k+1}, \nabla \boldsymbol{v}_h) - (p_h^{n+1,k+1}, \nabla\cdot \boldsymbol{v}_h) - \frac{1}{\rho}\left\langle \boldsymbol{j}_h^{n+1,k+1}\times \boldsymbol{B}, \boldsymbol{v}_h \right\rangle \\
&\quad + \left\langle \boldsymbol{u}_h^{n+1,k}\cdot\nabla \boldsymbol{v}_h + \nu\Delta \boldsymbol{v}_h, \tau_1^{n+1,k}\boldsymbol{R}_{h,u}^{n+1,k+1} \right\rangle_h + \left\langle \nabla\cdot \boldsymbol{v}_h, \tau_2^{n+1,k} R_{h,p}^{n+1,k+1} \right\rangle_h \\
&\quad - \left\langle \frac{1}{\rho}(\boldsymbol{v}_h\times \boldsymbol{B}), \tau_3^{n+1,k}\boldsymbol{R}_{h,j}^{n+1,k+1} \right\rangle_h = \langle \boldsymbol{f}^{\,n+1}, \boldsymbol{v}_h \rangle, \\
&(q_h, \nabla\cdot \boldsymbol{u}_h^{n+1,k+1}) + \left\langle \nabla q_h, \tau_1^{n+1,k}\boldsymbol{R}_{h,u}^{n+1,k+1} \right\rangle_h = 0, \\
&\frac{1}{\rho\sigma}(\boldsymbol{j}_h^{n+1,k+1}, \boldsymbol{k}_h) + \frac{1}{\rho}(\nabla \phi_h^{n+1,k+1}, \boldsymbol{k}_h) - \frac{1}{\rho}(\boldsymbol{u}_h^{n+1,k+1}\times \boldsymbol{B}, \boldsymbol{k}_h) \\
&\quad - \left\langle \frac{1}{\rho}(\boldsymbol{k}_h\times \boldsymbol{B}), \tau_1^{n+1,k}\boldsymbol{R}_{h,u}^{n+1,k+1} \right\rangle_h - \left\langle \frac{1}{\rho\sigma}\boldsymbol{k}_h, \tau_3^{n+1,k}\boldsymbol{R}_{h,j}^{n+1,k+1} \right\rangle_h + \left\langle \frac{1}{\rho}\nabla\cdot \boldsymbol{k}_h, \tau_4^{n+1,k} R_{h,\phi}^{n+1,k+1} \right\rangle_h = 0, \\
&-\frac{1}{\rho}(\nabla\psi_h, \boldsymbol{j}_h^{n+1,k+1}) + \left\langle \frac{1}{\rho}\nabla\psi_h, \tau_3^{n+1,k}\boldsymbol{R}_{h,j}^{n+1,k+1} \right\rangle_h = 0,
\end{aligned}
$$

where the expression of the residuals is,

$$
\begin{aligned}
&\boldsymbol{R}_{h,u} := \delta_t \boldsymbol{u}_h + \boldsymbol{a}\cdot\nabla \boldsymbol{u}_h - \nu\Delta \boldsymbol{u}_h + \nabla p_h - \frac{1}{\rho}(\boldsymbol{j}_h\times \boldsymbol{B}) - \boldsymbol{f}, \\
&R_{h,p} := \nabla\cdot \boldsymbol{u}_h, \\
&\boldsymbol{R}_{h,j} := \frac{1}{\rho\sigma}\boldsymbol{j}_h + \frac{1}{\rho}\nabla\phi_h - \frac{1}{\rho}(\boldsymbol{u}_h\times \boldsymbol{B}), \\
&R_{h,\phi} := \frac{1}{\rho}\nabla\cdot \boldsymbol{j}_h,
\end{aligned}
$$

with $\boldsymbol{a} = \boldsymbol{u}_h^{n+1,k}$. The superscript in the residuals and the stabilization parameters denotes the unknown with which they are evaluated.

6. Numerical experimentation

6.1. Comparison between monolithic solvers and uncoupling schemes

There exist several strategies to solve the linear system of equations resulting from the final numerical scheme written in Section 5. On one hand, the problem can be stated in a monolithic way, leading to a linear system of equations that includes all the problem unknowns. We can state the problem in an algebraic setting as:

$$
\begin{pmatrix} A_{uu} & A_{uj} \\ A_{ju} & A_{jj} \end{pmatrix} \begin{pmatrix} \mathbf{u} \\ \mathbf{j} \end{pmatrix} = \begin{pmatrix} \mathbf{f}_u \\ \mathbf{f}_j \end{pmatrix}
$$

where the arrays $\mathbf{u}$ and $\mathbf{j}$ include the fluid and electromagnetic unknowns respectively. Using this splitting of the unknowns, we have written the system matrix and force vector in a block fashion. So, the block matrices A_{uj} and A_{ju} represent the coupling terms. In a compact form, the problem can simply be written as $A\mathbf{x} = \mathbf{f}$.

The coupled linear system can be solved with our preferred solver and preconditioner. A flexible and quite robust preconditioner P consists of an incomplete LU (ILU) factorization of the system matrix, in one of its multiple versions (see, e.g., [27]). So, e.g., the left-preconditioned system reads as $P^{-1}A\mathbf{x} = P^{-1}\mathbf{f}$. Since we are dealing with a non-symmetric matrix A, the GMRES Krylov iterative solver is a good choice. Therefore, the coupling between subproblems is transferred to an effective solver and the off-diagonal coupling matrices are also present in the preconditioner P. Other effective preconditioners for saddle-point problems are block preconditioners based on Schur complement approximations together with multigrid iterations; we refer to [15] for a detailed discussion in the frame of Stokes and Navier–Stokes problems.

On the other hand, there exists also the option to consider a segregated approach to the problem, i.e. sending the coupling terms to the right hand side and considering separated fluid and electromagnetic solvers. In this case, the coupling is performed via external iterations. This approach is nothing but a block-matrix splitting technique with stationary iterations. Let us consider the splitting $A = P - R$, where P is the preconditioner and R the residual matrix. Stationary (Richardson) iterations read as

$$
P\mathbf{x}^{k+1} = R\mathbf{x}^k + \mathbf{f}, \quad \text{or equivalently} \quad \mathbf{x}^{k+1} = \mathbf{x}^k + P^{-1}(\mathbf{f} - A\mathbf{x}^k).
$$

Two typical preconditioners that decouple fluid and electromagnetic computations at the preconditioner level are the block-Jacobi (bJ) and block-Gauss–Seidel (bGS) preconditioners:

$$
P_{\mathrm{bJ}} = \begin{pmatrix} A_{uu} & 0 \\ 0 & A_{jj} \end{pmatrix} \quad \text{and} \quad P_{\mathrm{bGS}} = \begin{pmatrix} A_{uu} & 0 \\ A_{ju} & A_{jj} \end{pmatrix}.
$$

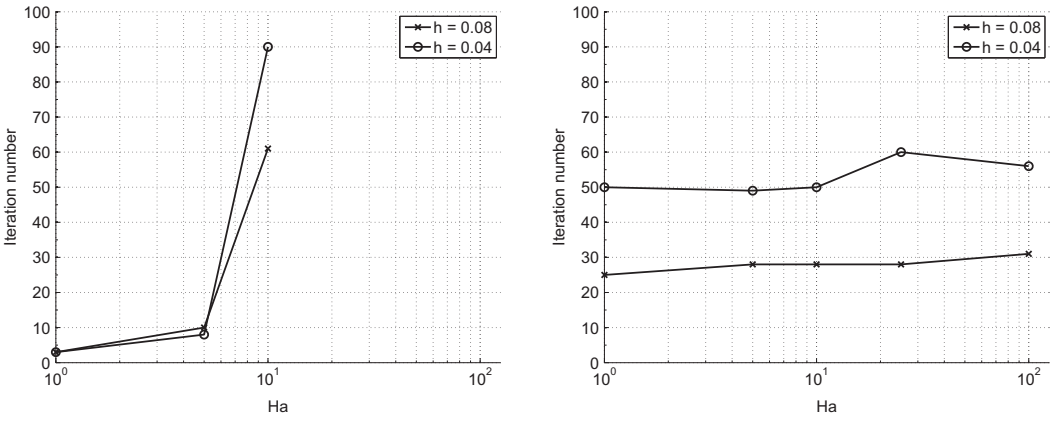

Fig. 1. Number of iterations depending on the Hartmann number Ha.

This *segregated* approach has two weak points: the preconditioner is independent from the coupling terms and the coupling iterations do not involve any orthogonalization (minimization) procedure. So, the convergence of the method is expected to deteriorate as the coupling becomes more important. It is well-known in other settings that this methodology is ill-posed for strongly coupled problems. As long as the coupling terms increase, the convergence becomes slower or it simply diverges (see e.g., [4,32,7] for detailed discussions in the fluid–structure framework).

These two different approaches to solve the coupled problem have been compared for the Hunt's example; see Section 6.3 for a complete definition of the problem. In this study, two meshes, the coarsest one consisting of 2028 nodes and 7500 linear tetrahedral elements and the finest one with 7803 nodes and 30000 linear tetrahedral elements, have been used. The problem has been solved for different values of the Hartmann number Ha = 1, 5, 10, 25, 100, where

$$\mathrm{Ha} = BL\sqrt{\frac{\sigma}{\rho\nu}},$$

L being a characteristic length of the problem and B the norm of the externally applied magnetic field. Larger values of Ha mean stronger coupling effects.

The method selected to solve the problem in a monolithic way is the GMRES method, preconditioning the matrix of the system using an ILU factorization; the built-in MATLAB implementation of both schemes has been used. In particular, we have used the ILUTP factorization, setting the drop tolerance to 10^{-4}. The GMRES residual tolerance has been set to 10^{-8}. For the Richardson iterations, we have considered the bGS preconditioner; the stopping criteria is based on the magnitude of the residual, with a tolerance of 10^{-8}.

Fig. 1 shows the number of iterations needed to achieve a converged solution in terms of the corresponding tolerances for both approaches and both discretizations. It is very clear in Fig. 1(a) that the Richardson-bGS approach is very sensitive to the magnitude of the coupling. When the coupling effects are low, for Ha = 1, 5, the Richardson method converges quickly to the coupled solution. However, when the coupling is stronger, for Ha = 10, the number of iterations is much larger; the algorithm is not able to converge for Ha = 25, 100. On the other hand, the monolithic approach to solve the coupled problem has a much better behavior. The ILUTP-GMRES method is insensitive to the Ha number. Let us remark that the number of iterations presented for the Richardson-bGS method corresponds to external (coupling) iterations; we are not including the number of internal Krylov iterations needed for the evaluation of every subproblem. On the contrary, ILUTP-GMRES only include one iteration counter, and so, the iterations showed in Fig. 1(b) are the only iterations to be performed.

Despite these results, previous approaches to the inductionless MHD problem systematically used the $\boldsymbol{u} - \phi$ formulation which uncouples the hydrodynamic and magnetic problems and solves the electric potential via a Poisson problem. Therefore, this solving strategy involves Richardson-bGS or Richardson-bJ iterations, probably together with relaxation or line search techniques (see [6,21,24,25]).[2] This approach is effective for low Ha, but inappropriate for large Ha numbers, as those encountered in TBMs simulations. As a result, TBM simulations cannot be properly addressed when using $\boldsymbol{u} - \phi$ formulations. These results justify our approach to the inductionless MHD problem. Since real applications in fusion reaction technology involve Ha numbers of the order of $10^3 - 10^4$, a monolithic approach should be clearly favoured. Furthermore, as far as we know, there are no compatible finite element formulations for both sub-problems (Stokes and Darcy type sub-systems), that is to say,

[2] Alternatively, this approach can be casted in a transient framework, in which the coupling is treated explicitly; in this situation, the convergence problem related to strong coupling is passed to the time step size. Stable time marching schemes with explicit coupling will require time step sizes that go to zero as Ha increases.

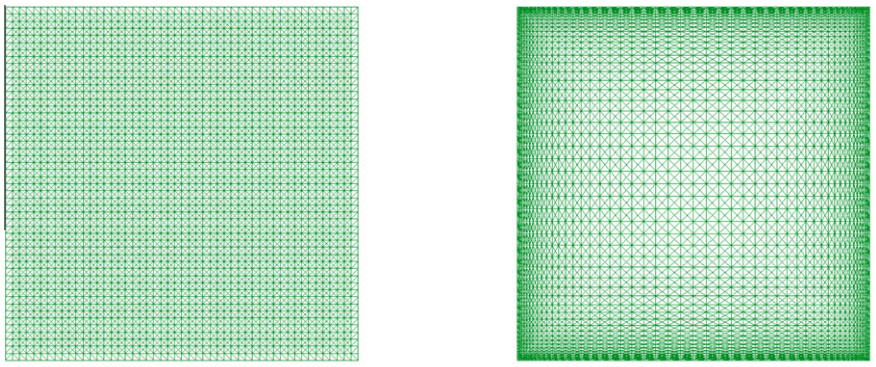

(a) Uniformly structured mesh

(b) Structured mesh but concentrating elements near the boundaries

Fig. 2. Mesh configurations.

elements that satisfy both inf-sup conditions (22) such that the bilinear forms associated to the primal variable are coercive in the kernel of the finite element subspaces for Stokes' and Darcy's problem (see [2] for a detailed discussion). So, our stabilized formulation is appealing, in the sense that it allows equal interpolation for the different unknowns (simplifying data-base structures, coupling terms implementation and reducing CPU cost) and the use of effective solvers for high Ha numbers.

6.2. Shercliff's case

The first numerical experiment that has been carried out is the simulation of the Shercliff's case. It corresponds to a fully developed flow in a channel with square section where both the Hartmann walls, which are the walls orthogonal to the external magnetic field direction, and the side walls, which are the walls parallel to the external magnetic field, are considered electrically insulating. The fluid flows with unidirectional velocity in the z-direction driven by a constant pressure gradient. The channel is exposed to an external magnetic field applied in the y-direction. This problem has an analytical solution in form of Fourier series that was developed by J. A. Shercliff [31]. A more appropriate version of this solution for the implementation in a computer can be found in [25] [3]. The formulae used in this work to compute the analytical solution and compare with the numerical approximation are explained in Appendix A.

This problem has a 2D behavior that has been simulated setting as the computational domain a slice of the channel of width 1/100 times the section sides. The boundary conditions at the inflow and outflow sections have been set as periodic boundary conditions to enforce the situation of fully developed flow. Therefore, the constant pressure gradient that drives the liquid has to be set as an external body force. Its value can be computed as (see [23] for details)

$$\frac{\mathrm{d}p}{\mathrm{d}z} = \frac{KL^3}{\rho\nu^2 \mathrm{Re}},$$

with

$$K = \frac{\mathrm{Ha}}{1 - 0.825\mathrm{Ha}^{-1/2} - \mathrm{Ha}^{-1}}, \qquad \mathrm{Re} = \frac{UL}{\nu},$$

where U is a characteristic velocity of the fluid. Every physical property of the problem, that is, density, viscosity and electrical conductivity has been set equal to one. In this way, the Hartmann number Ha is equal to the norm of the external magnetic field. Several meshes have been used to perform the computations. The coarsest consists of 2028 nodes and 7500 tetrahedral elements whereas the finest consists of 121203 nodes and 480000 tetrahedral elements. Furthermore, two different configurations of meshes have been considered, a uniformly structured one and a structured one but concentrating the elements near the boundaries. Fig. 2 shows the two different configurations for a mesh of 30000 elements.

The first simulation has been performed for Ha = 10 and Re = 10. Fig. 3 shows the velocity field and the current paths obtained using a mesh of 30603 nodes and 120000 tetrahedral elements.

The second simulation is for a test problem with Ha = 100 and Re = 10. In this case, the uniformly structured meshes do not lead to a proper solution because the Hartmann layer is much thinner than the mesh size h. Therefore, this case has been solved with meshes concentrating elements near the boundaries. The results for a mesh of 30603 nodes and 120000 tetrahedral elements are shown in Fig. 4.

[3] There are some typographical errors in two of the formulae in [25].

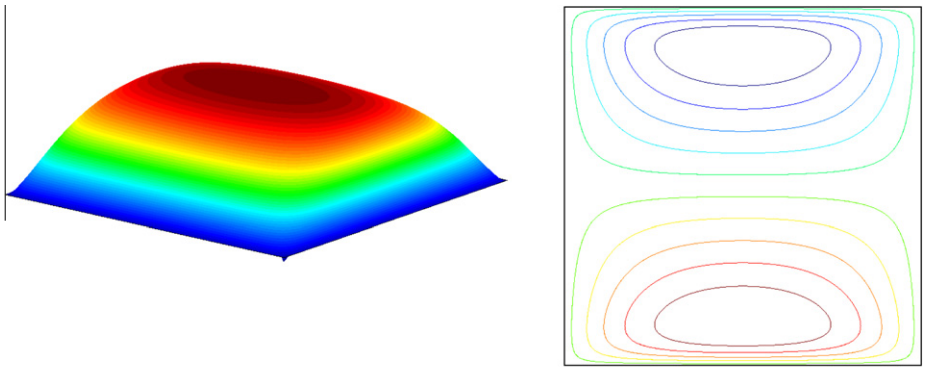

(a) Velocity field (b) Current paths

Fig. 3. Shercliff's case: Ha = 10, Re = 10.

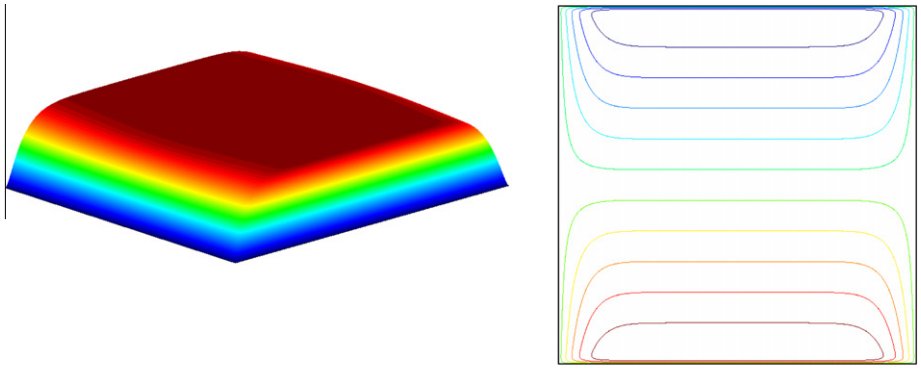

(a) Velocity field (b) Current paths

Fig. 4. Shercliff's case: Ha = 100, Re = 10.

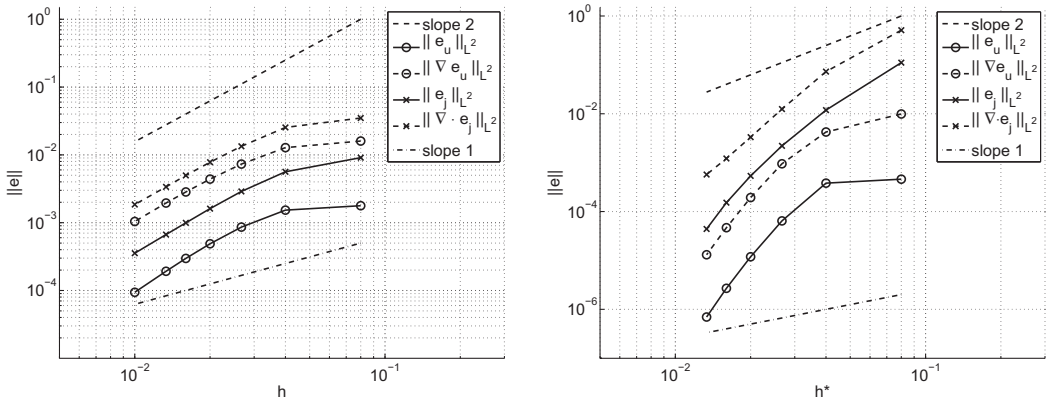

(a) Mesh in Fig. 2(a) with Ha=10 (b) Mesh in Fig. 2(b) with Ha=100

Fig. 5. Shercliff's case convergence rates.

Fig. 5 shows the convergence study of both Ha = 10 and Ha = 100 cases depending on the mesh size h in a logarithmic scale. Note that the mesh size for the meshes with element concentration is not constant. Therefore, the results have been plotted related to an equivalent mesh size h^* which corresponds to the same number of degrees of freedom than a uniformly

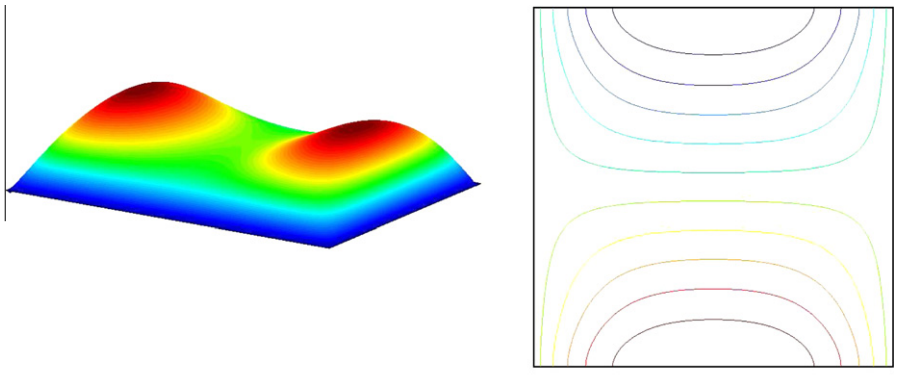

(a) Velocity field (b) Current paths

Fig. 6. Hunt's case: Ha = 10, Re = 10.

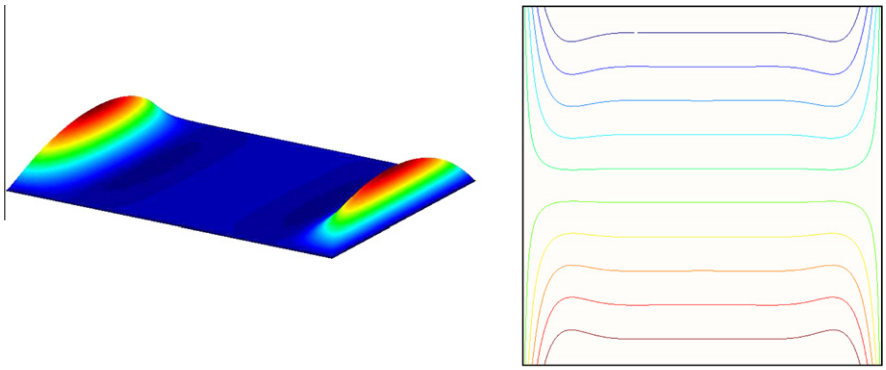

(a) Velocity field (b) Current paths

Fig. 7. Hunt's case: Ha = 100, Re = 10.

structured mesh. The values shown in this study correspond to the L^2-norm of the error in the velocity $\|\boldsymbol{e}_u\|$, the velocity gradient $\|\nabla\boldsymbol{e}_u\|$, the current density $\|\boldsymbol{e}_j\|$ and the divergence of the current density $\|\nabla\cdot\boldsymbol{e}_j\|$. It can be clearly seen that in both cases, Ha = 10 and Ha = 100, the convergence rates are very good for every computed error. Actually, the convergence rates for the velocity gradient and the divergence of the current density are higher than the theoretical value; similar behavior has been found in [2] for the Darcy problem.

6.3. Hunt's case

The next test problem is Hunt's case. It corresponds to a fully developed flow in a channel with square section where the Hartmann walls are perfectly conducting and the side walls are electrically insulated. Similarly to Shercliff's case, this problem has an analytical solution (see Appendix B).

This problem has a similar 2D behavior to the one for Shercliff's case. We have used the same computational domain, that is, a slice of channel of width 1/100 times the section sides with periodic conditions at the inflow and outflow sections. Therefore, the constant pressure gradient that drives the flow has to be set as an external body force. Its value can be computed with a slightly different formula from Shercliff's case as (see [23] for details)

$$\frac{\mathrm{d}p}{\mathrm{d}z} = \frac{KL^3}{\rho\nu^2\mathrm{Re}}, \quad \text{where} \quad K = \frac{\mathrm{Ha}}{1 - 0.95598\mathrm{Ha}^{-1/2} - \mathrm{Ha}^{-1}}.$$

Every physical property involved in the calculation has been set equal to one. Therefore, the Hartmann number is computed directly as the norm of the external magnetic field. The meshes used to solve this problem and obtain the convergence rates are the same meshes that were used in the previous case.

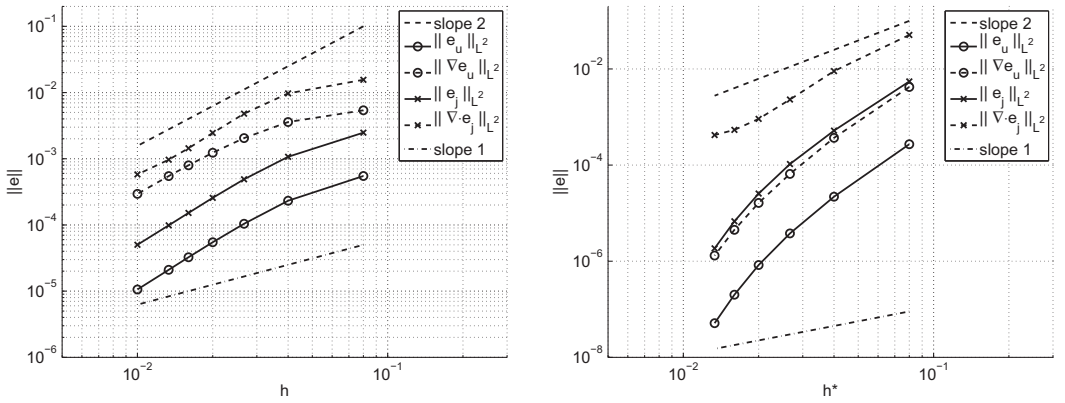

(a) Mesh in Fig. 2(a) with Ha=10 (b) Mesh in Fig. 2(b) with Ha=100

Fig. 8. Hunt's case convergence rates.

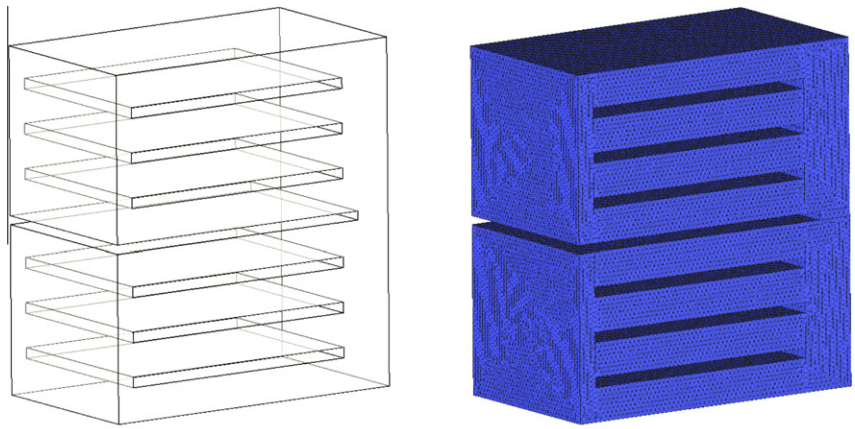

(a) HCLL blanket geometry (b) Computational mesh

Fig. 9. HCLL blanket configuration.

The same two simulations as in the Shercliff's case have been performed. The first one is a fluid with Ha = 10 and Re = 10. Fig. 6 shows the velocity field and the current paths solution of this problem when using a structured mesh of 30603 nodes and 120000 tetrahedral elements.

The second simulation corresponds to a fluid flowing with Ha = 100 and Re = 10. Fig. 7 shows the velocity distribution and the current paths obtained with a mesh of 30603 nodes and 120000 tetrahedral elements but concentrating the elements near the boundaries to capture the Hartmann layers.

Fig. 8 shows the convergence rates obtained for both Ha = 10 and Ha = 100 cases in a logarithmic scale. Again, for the meshes with element concentration, an equivalent mesh size h^* has been used. The quantities shown are: the L^2-norm of the error in the velocity $\|\boldsymbol{e}_u\|$, the velocity gradient $\|\nabla\, \boldsymbol{e}_u\|$, the current density $\|\boldsymbol{e}_j\|$ and the divergence of the current density $\|\nabla \cdot \boldsymbol{e}_j\|$. Again, the results show that in both cases the convergence rates are very good. Furthermore, the errors in the velocity gradient and the divergence of the current density also present a superconvergent behavior in relation to the theoretical expected value.

6.4. HCLL test blanket

The helium cooled lead lithium (HCLL) blanket is a liquid metal blanket concept developed in the framework of the European breeding blanket programme for a DEMO reactor to be tested in ITER (see the web site <www.iter.org>). Fig. 9(a) shows the geometry considered as computational domain, see [21,22] for details. It consists of a U-shaped channel which measures 360 mm in its longitudinal direction (x-axis). The total height is 39 mm (z-axis) divided into two subchannels of 190 mm and a transition zone of 1 mm. The section width (y-axis) is 206. mm. In every one of the subchannels, there are 3 cooling plates whose dimensions are $280 \times 206.5 \times 12$ mm.

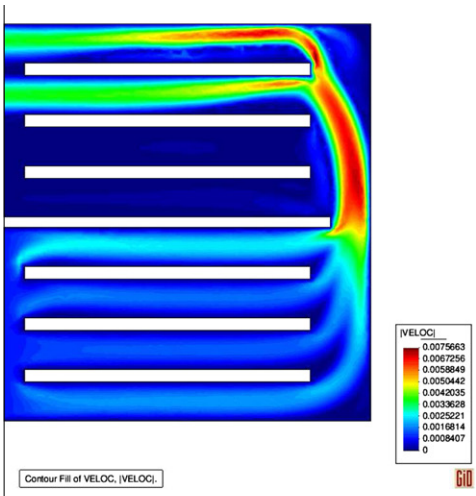

(a) Velocity norm

(b) Velocity field

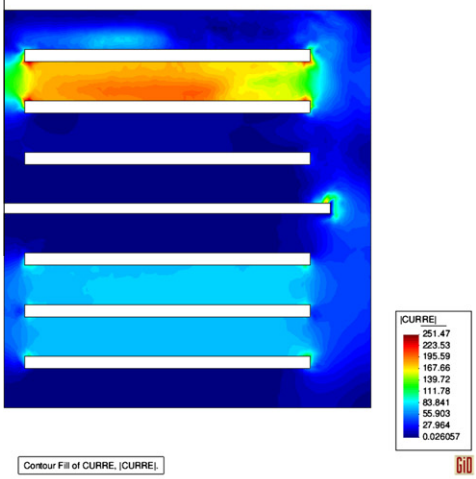

(c) Current norm

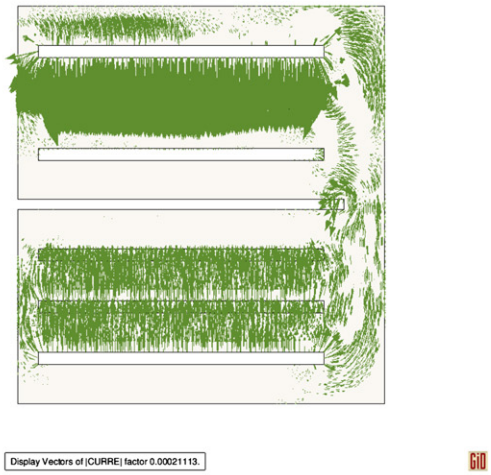

(d) Current field

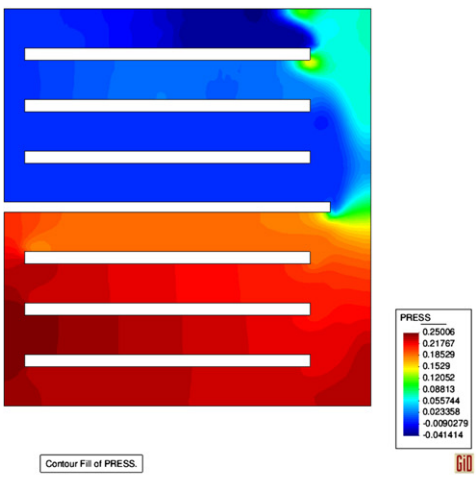

(e) Pressure

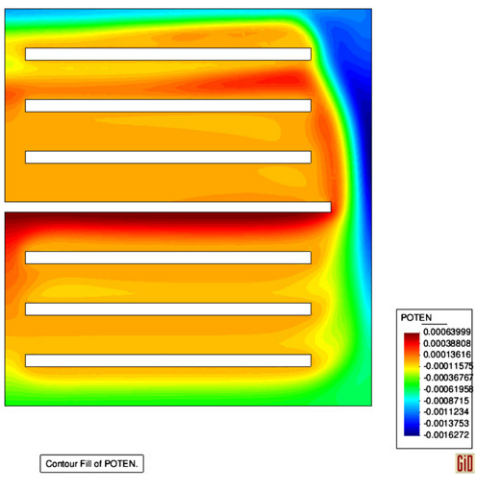

(f) Electric potential

Fig. 10. Results in section $y = 0.103$ m.

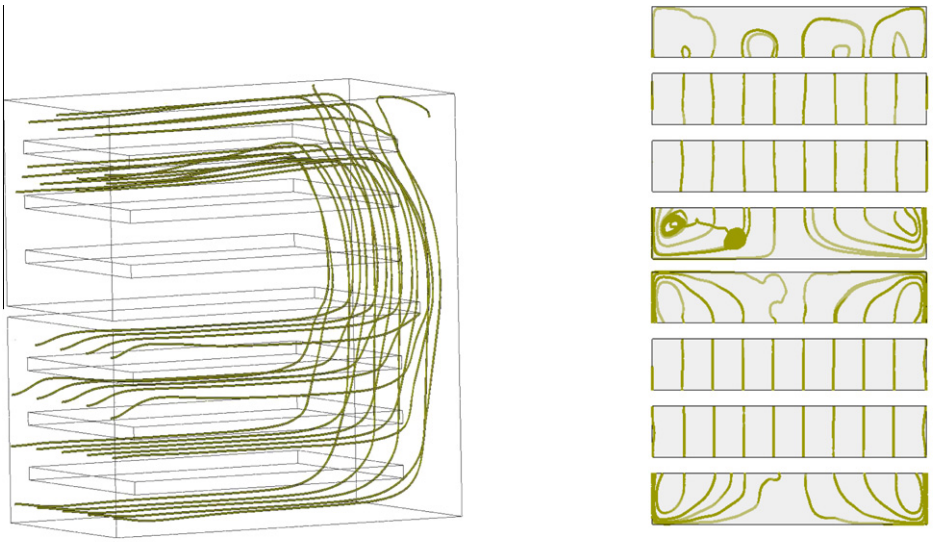

(a) Velocity streamlines

(b) Current density streamlines at section $x = 0.150$ m

Fig. 11. Velocity field and current density field streamlines.

Fig. 9(b) shows the mesh generated to perform the calculations. It consists of 266,072 nodes and 1,417,435 linear tetrahedral elements. This mesh leads to 2, 128, 576 degrees of freedom.

The physical properties of the eutectic Pb-17Li fluid have been considered to be constant. The adopted values in this work are: fluid density $\rho = 9.2 \times 10^3$ kg/m^3, fluid viscosity $\nu = 1.4 \times 10^{-7}$ m^2/s and fluid electrical conductivity $\sigma = 7.4 \times 10^3$ $1/\Omega$ m (see [6,14] for more details). The external magnetic field applied to the fluid has a value of 10 T and has a direction in the y-axis, $\boldsymbol{B} = (0, 10, 0)$T. Considering that the characteristic magnetic length is half the length of the side walls, $L = 0.103$ m, the Hartmann number associated to this flow is Ha = 2470.

The hydrodynamic boundary conditions have been set as $\boldsymbol{u} = \boldsymbol{0}$ at the walls, both the external walls and the cooling plates, $\boldsymbol{u} = (0.001, 0, 0)$ m/s at the inlet, which corresponds to the bottom subchannel, and free condition at the outlet, the top subchannel.

On the other hand, the magnetic boundary conditions have been set as perfectly insulating material in the exterior walls, that is $\boldsymbol{j} \cdot \boldsymbol{n} = 0$, and perfectly conducting material in the cooling plates, which corresponds to $\boldsymbol{j} \times \boldsymbol{n} = \boldsymbol{0}$.

The solution to this problem converges to a stationary solution. In Fig. 10 there have been plotted the solutions in the plane $y = 0.103$ m. Those graphics show the longitudinal behavior of the flow in the x-direction. The velocity field shows clearly that the distribution of the cooling plates in the top subchannel is not optimal because almost the entire flow takes place in the top part of the subchannel whereas in the bottom part the fluid has velocity equal to zero. Furthermore, the high values of the velocity near the top part of the top subchannel results on higher values of the current density in the same zone, instead of the distribution that could be expected, similar to the Shercliff's case solution, which actually is the solution in the bottom subchannel.

Fig. 11(a) shows the streamlines of the velocity field. It is clearly seen how the fluid entering the blanket from the inlet surface goes to the outlet through only the top 2 subchannels, leaving the bottom 2 subchannels of the upper module with almost zero velocity. On the other hand, Fig. 11(b) displays the current density streamlines in section $x = 0.150$ m. The streamlines in the bottom module reproduce almost perfectly the streamlines of Shercliff's case where both the Hartmann and side walls are perfectly insulating. However, the top module behavior is different. The velocity field concentrating in the top 2 subchannels produces a different distribution of the current density field.

7. Conclusions

In this paper, a numerical formulation to solve the inductionless MHD equations that consists of a stabilized FE method has been presented. Its design is based on the variational multiscale framework which is derived from a splitting of the unknown into two parts, a FE component and a subscale that corresponds to the part of the unknown that cannot be captured by the discretization. The crucial point in this approach resides in the subscale approximation.

The most important aspects of this formulation are that it allows to use equal interpolation for all the unknowns without having to satisfy the compatibility conditions. Furthermore, it is stable and optimally convergent in a norm that is meaningful for every value of the physical parameters of the fluid.

Another key point of this formulation is the monolithic approach for solving the problem instead of the possibility of uncoupling the global problem by solving a Laplacian equation for the electric potential. This latter option needs a block iteration algorithm to converge to the coupled solution but there exists no guarantee that it will converge to the solution nor the number of iterations needed in case it converges.

The approximation of the subscales leads to the introduction of some stabilization parameters that need to be proposed. An interesting point of this work is that these parameters have been designed based on the stability and convergence analysis of the method.

The time integration and linearization of the problem considered here is the simplest possible which leads to a method easy to implement but without losing any robustness and convergence properties. The numerical experimentation presented in this article validates these statements and the theoretical development of the method.

Acknowledgements

This work has been partially supported by the *Consolider-Ingenio* project TECNOFUS, Ref. CSD2008–00079, from the Spanish Ministry of Science and Innovation. Furthermore, R. Planas would like to aknowledge the support received from the *Universitat Politècnica de Catalunya (UPC)* and from the *Col.legi d'Enginyers de Camins, Canals i Ports de Catalunya.*

Appendix A. Shercliff's analytical solution

Let the side walls be of length $2a$, the Hartmann walls of length $2b$ and $l = b/a$. The Hartmann walls are considered to have arbitrary conductivity with $d_B = (t_w\sigma_w)/(a\sigma)$, where σ_w is the conductivity of the wall, t_w its thickness and σ the conductivity of the fluid. The analytical solution was given by Hunt [20] as a Fourier series in $\xi = x/a \in [-l, l]$ and $\eta = y/a \in [-1, 1]$. The z-component of the velocity is written as

$$u_z = \frac{V}{\mu}\left(-\frac{\partial p}{\partial z}\right)a^2, \quad \text{where } V = \sum_{k=0}^{\infty} \frac{2(-1)^k \cos(\alpha_k \xi)}{l\alpha_k^3}(1 - V2 - V3), \tag{42}$$

for

$$V2 = \frac{\left(d_B r_{2k} + \frac{1-\exp(-2r_{2k})}{1+\exp(-2r_{2k})}\right)\frac{\exp(-r_{1k}(1-\eta))+\exp(-r_{1k}(1+\eta))}{2}}{\frac{1+\exp(-2r_{1k})}{2}d_B N + \frac{1-\exp(-2(r_{1k}+r_{2k}))}{1+\exp(-2r_{2k})}},$$

$$V3 = \frac{\left(d_B r_{1k} + \frac{1-\exp(-2r_{1k})}{1+\exp(-2r_{1k})}\right)\frac{\exp(-r_{2k}(1-\eta))+\exp(-r_{2k}(1+\eta))}{2}}{\frac{1+\exp(-2r_{2k})}{2}d_B N + \frac{1-\exp(-2(r_{1k}+r_{2k}))}{1+\exp(-2r_{1k})}},$$

and

$$N = (\mathrm{Ha}^2 + 4\alpha_k^2)^{1/2}, \quad r_{1k}, r_{2k} = \frac{1}{2}\left(\pm\mathrm{Ha} + (\mathrm{Ha}^2 + 4\alpha_k^2)^{1/2}\right), \quad \alpha_k = \left(k + \frac{1}{2}\right)\frac{\pi}{l}.$$

On the other hand, the current density components j_x and j_y are $j_x = \frac{\partial H_z}{\partial y}$ and $j_y = -\frac{\partial H_z}{\partial x}$ for

$$H_z = \frac{H}{\mu^{1/2}}\left(-\frac{\partial p}{\partial z}\right)a^2\sigma^{1/2} \quad \text{where } H = \sum_{k=0}^{\infty} \frac{2(-1)^k \cos(\alpha_k \xi)}{l\alpha_k^3}(H2 - H3), \tag{43}$$

for

$$H2 = \frac{\left(d_B r_{2k} + \frac{1-\exp(-2r_{2k})}{1+\exp(-2r_{2k})}\right)\frac{\exp(-r_{1k}(1-\eta))-\exp(-r_{1k}(1+\eta))}{2}}{\frac{1+\exp(-2r_{1k})}{2}d_B N + \frac{1-\exp(-2(r_{1k}+r_{2k}))}{1+\exp(-2r_{2k})}},$$

$$H3 = \frac{\left(d_B r_{1k} + \frac{1-\exp(-2r_{1k})}{1+\exp(-2r_{1k})}\right)\frac{\exp(-r_{2k}(1-\eta))-\exp(-r_{2k}(1+\eta))}{2}}{\frac{1+\exp(-2r_{2k})}{2}d_B N + \frac{1-\exp(-2(r_{1k}+r_{2k}))}{1+\exp(-2r_{1k})}}.$$

V_z, j_x and j_y are precisely the analytical solution of the problem. Note that in the Shercliff's case the Hartmann walls are perfectly insulating, and therefore $d_B = 0$ in the above formulae. Note also that the formulae in [20] have been written in terms of exponential functions to allow its computation in a computer. The original formulae in terms of hyperbolic functions is not suitable for computing at high values of the Hartmann number.

Appendix B. Hunt's analytical solution

Hunt's problem has an analytical solution in the form of Fourier series that can be found in an article from J.C.R. Hunt [20]. The analytical solution is computed using the formulae (42) and (43). In this case, the Hartmann walls are perfectly conduct-

ing and therefore $d_B \to \infty$. Thus, the modifications in the formulae (42) and (43) for Hunt's case consist of taking the limit $d_B \to \infty$ in the Fourier series:

$$V2 = \frac{r_{2k}}{N} \cdot \frac{\exp(-r_{1k}(1-\eta)) + \exp(-r_{1k}(1+\eta))}{1+\exp(-2r_{1k})},$$
$$V3 = \frac{r_{1k}}{N} \cdot \frac{\exp(-r_{2k}(1-\eta)) + \exp(-r_{2k}(1+\eta))}{1+\exp(-2r_{2k})},$$
$$H2 = \frac{r_{2k}}{N} \cdot \frac{\exp(-r_{1k}(1-\eta)) - \exp(-r_{1k}(1+\eta))}{1+\exp(-2r_{1k})},$$
$$H3 = \frac{r_{1k}}{N} \cdot \frac{\exp(-r_{2k}(1-\eta)) - \exp(-r_{2k}(1+\eta))}{1+\exp(-2r_{2k})}.$$

References

[1] S. Badia, R. Codina, Algebraic pressure segregation methods for the incompressible Navier–Stokes equations, Archives of Computational Methods in Engineering 15 (2008) 343–369.
[2] S. Badia, R. Codina, Unified stabilized finite element formulations for the Stokes and the Darcy problems, SIAM Journal on Numerical Analysis 47 (3) (2009) 1971–2000.
[3] S. Badia, R. Codina, J.V. Gutiérrez-Santacreu, Long-term stability estimates and existence of a global attractor in a finite element approximation of the Navier–Stokes equations with numerical sub-grid scale modeling, SIAM Journal on Numerical Analysis 48 (3) (2010) 1013–1037.
[4] S. Badia, A. Quaini, A. Quarteroni, Modular vs. non-modular preconditioners for fluid-structure systems with large added-mass effect, SIAM Journal on Numerical Analysis 197 (49-50) (2008) 4216–4232.
[5] F. Brezzi, M. Fortin, Mixed and Hybrid Finite Element Methods, Springer Verlag, 1991.
[6] L. Bühler, Liquid metal magnetohydrodynamics for fusion blankets, in: R. Moreau, S. Molokov, H.K. Moffat (Eds.), Magnetohydrodynamics. Historical Evolution and Trends, Springer, 2007, pp. 171–194.
[7] P. Causin, J.F. Gerbeau, F. Nobile, Added-mass effect in the design of partitioned algorithms for fluid-structure problems, SIAM Journal on Numerical Analysis 194 (42-44) (2005) 4506–4527.
[8] R. Codina, On stabilized finite element methods for linear systems of convection–diffusion-reaction equations, SIAM Journal on Numerical Analysis 188 (2000) 61–82.
[9] R. Codina, Stabilized finite element approximation of transient incompressible flows using orthogonal subscales, SIAM Journal on Numerical Analysis 191 (2002) 4295–4321.
[10] R. Codina, S. Badia, On some pressure segregation methods of fractional-step type for the finite element approximation of incompressible flow problems, SIAM Journal on Numerical Analysis 47 (2006) 2900–2918.
[11] R. Codina, N. Hernández, Approximation of the thermally coupled MHD problem using a stabilized finite element method, Journal of Computational Physics 230 (2011) 1281–1303.
[12] R. Codina, N. Hernández, Stabilized finite element approximation of the stationary MHD equations, Computational Mechanics 38 (2006) 344–355.
[13] R. Codina, J. Principe, O. Guasch, S. Badia, Time dependent subscales in the stabilized finite element approximation of incompressible flow problems, SIAM Journal on Numerical Analysis 196 (2007) 2413–2430.
[14] E. Mas de les Valls, L.A. Sedano, L. Batet, I. Ricapito, A. Aiello, O. Gastaldi, F. Gabriel, Lead–lithium eutectic material database for nuclear fusion technology, Journal of Nuclear Materials 376 (2008) 353–357.
[15] H. Elman, D. Silvester, A. Wathen, Finite Elements and Fast Iterative Solvers, Oxford Science Publications, 2005.
[16] A. Ern, J.L. Guermond, Theory and Practice of Finite Elements, Springer Verlag, 2004.
[17] J.F. Gerbeau, A stabilized finite element method for the incompressible magnetohydrodynamic equations, Numerische Mathematik 87 (2000) 83–111.
[18] T.J.R. Hughes, Multiscale phenomena: Green's function, the Dirichlet-to-Neumann formulation, subgrid scale models, bubbles and the origins of stabilized formulations, SIAM Journal on Numerical Analysis 127 (1995) 387–401.
[19] T.J.R. Hughes, L.P. Franca, G.M. Hulbert, A new finite element formulation for computational fluid dynamics: VIII. The Galerkin/least-squares method for advective-diffusive equations, SIAM Journal on Numerical Analysis 73 (1989) 173–189.
[20] J.C.R. Hunt, Magnetohydrodynamic flow in rectangular ducts, Journal of Fluid Mechanics 21 (1965) 577–590.
[21] C. Mistrangelo, Magnetohydrodynamic flow in a mock-up of a HCLL blanket. Part I. Numerical analysis, Technical Report FZKA 7312, Forschungszentrum Karlsruhe, (2008).
[22] C. Mistrangelo, L. Bühler, Influence of helium cooling channels on magnetohydrodynamic flows in the HCLL blanket, Fusion Engineering and Design 84 (2009) 1323–1328.
[23] U. Müller, L. Bühler, Magnetofluiddynamics in Channels and Containers, Springer, 2001.
[24] M.-J. Ni, R. Munipalli, P. Huang, N.B. Morley, M.A. Abdou, A current density conservative scheme for incompressible MHD flows at a low magnetic Reynolds number. Part I: On a rectangular collocated grid system, Journal of Computational Physics 227 (2007) 174–204.
[25] M.-J. Ni, R. Munipalli, P. Huang, N.B. Morley, M.A. Abdou, A current density conservative scheme for incompressible MHD flows at a low magnetic Reynolds number. Part II: On an arbitrary collocated mesh, Journal of Computational Physics 227 (2007) 205–228.
[26] J. Principe, R. Codina, F. Henke, The dissipative structure of variational multiscale methods for incompressible flows, SIAM Journal on Numerical Analysis 199 (2010) 791–801.
[27] Y. Saad, Iterative Methods for Sparse Linear Systems, PWS Publishing, Boston, MA, 1996.
[28] N. Ben Salah, A. Soulaimani, W.G. Habashi, A finite element method for magnetohydrodynamics, SIAM Journal on Numerical Analysis 190 (2001) 5867–5892.
[29] D. Schötzau, Mixed finite element methods for stationary incompressible magneto-hydrodynamics, Numerische Mathematik 96 (2004) 771–800.
[30] J.N. Shadid, R.P. Pawlowski, J.W. Banks, L. Chacón, P. T Lin, R.S. Tuminaro, Towards a scalable fully-implicit fully-coupled resistive MHD formulation with stabilized FE methods, Journal of Computational Physics 229 (2010) 7649–7671.
[31] J.A. Shercliff, Steady motion of conducting fluids in pipes under transverse magnetic fields, Proceedings of Cambridge Philosophical Society 49 (1953) 126–144.
[32] P. Le Tallec, J. Mouro, Fluid structure interaction with large structural displacements, SIAM Journal on Numerical Analysis 190 (2001) 3039–3067.